Space–Time Structure of Monsoon Interannual Variability

PASCAL TERRAY

Laboratoire de Météorologie Dynamique du CNRS, Ecole Polytechnique, France

(Manuscript received 14 May 1994, in final form 11 May 1995)

ABSTRACT

The analysis of corrected ship reports [sea level pressure (SLP), sea surface temperature (SST), air temperature (AT)] and corrected land data (SLP, AT, rainfall) in the Indian sector reveals the existence of two low-frequency modes of monsoon variability during the 1900–1970 period.

- A definite biennial (B) mode exists on the SLP fields. This B oscillation is unambiguously linked with a southwest–northeast SLP anomaly gradient. During the summer monsoon, the B SLP pattern can be interpreted as an expansion/contraction of the monsoon activity since this mode is strongly coupled with rainfall variations over peninsular India.
- A strong low-frequency (LF) mode with period spanning 4–6 years is also seen on SLP fields over the Indian Ocean and subcontinent. The variance associated with this band is typically more important than the one observed for the B mode, and its spatial mark is also strikingly different since it is linked with a global pattern of variation. This mode has also a strong influence on the Indian summer rainfall fluctuations, particularly on the Ghats and in the Indo-Gangetic plains.

The amplitude of these oscillations varies widely during the 1900–1970 period. The LF mode is well defined during 1900–1923 and 1947–1970. There is a tendency for the energy associated with the B mode to decrease on the land while it increases over the Indian Ocean during the whole 1900–1970 interval.

Although these two timescales exist also on SST fields, cross-spectral analysis shows that ocean–atmosphere interactions are much stronger at the B timescale. This result stresses the B nature of the monsoon system.

The existence of these interannual signals in the Indian areas where the annual cycle is so strong raises difficult problems: How can climatic anomalies persist for several years in spite of strong seasonality? Or, still more intriguing, how can be explained the persistence of climatic anomalies during one year and the appearance of opposite sign climatic anomalies in the following year for the B mode? A composite analysis has suggested an explanation for this last problem: SST anomalies produced by exceptional summer monsoons can indeed persist during the whole winter and exert an influence on the next summer monsoon.

1. Introduction

The Indian summer monsoon (ISM) rainfall from June to September has a great impact on the economy of India and neighboring countries. It is then not surprising that the interannual variability of ISM has received continued study over the decades since the pioneering work of Blanford (1884).

Until recently, most of the studies have focused on the relationships between ISM rainfall and the El Niño–Southern Oscillation (ENSO) phenomenon (Walker 1923; Rasmusson and Carpenter 1983; Shukla and Paolino 1983; Parthasarathy and Pant 1985). Collectively, these works and many others have demonstrated that the two phenomena are strongly coupled. However, these strong links have only a limited use in foreshadowing the monsoon since ISM rainfall anomalies anticipate ENSO fluctuations (Elliott and Angell 1987). Thus, it cannot be expected that the Southern Oscillation (SO) could account for most of ISM variability.

Despite pervasive evidence of the great impact of ISM on low-frequency variability of the global climate system (Yasunari 1991), not much information is available to examine the nature and timescales of meteorological surface parameters over the Indian Ocean and their links with ISM rainfall.

In particular, whether or not Indian Ocean sea surface temperature (SST) anomalies are simply passive anomalies forced by the monsoon circulation is still unclear. Shukla and Misra (1977) show weak positive correlations between monthly SST over the Arabian Sea and rainfall over India. Weare (1979) finds the opposite: a warmer Arabian Sea is associated with decreased ISM rainfall. After removing some biases in the SST data, Shukla (1987) finds that heavy (deficient) rainfall is followed by negative (positive) SST anomalies but that the magnitude of the SST anomalies for the premonsoon months is small and insignificant. Joseph and Pillai (1984) obtain the same results. On

Corresponding author address: Dr. Pascal Terray, 30, Rue de Milly, 77930 Perthes, France.

the contrary, the studies of Wu and Hastenrath (1986) and Rao and Goswami (1988) suggest that warmer Arabian Sea temperatures during the premonsoon season are significantly associated with increased ISM rainfall. Finally, Ramesh Babu et al. (1989) find the opposite of Rao and Goswami in the sense that "monsoon activity at the west coast of India is more likely to be less when abnormal premonsoonal warming takes place in the eastern Arabian Sea." In summary, there is a large discrepancy between the results of the various investigators, at least part of which can be attributed to the bad quality of SST data over the Indian Ocean (Terray 1994).

In the same manner, past works have not established conclusively what are the fundamental timescales of climate interannual variability over the Indian Ocean, if any. Moreover, it is not known if the significant relationships between ISM rainfall and the surface parameters over the Indian Ocean during ISM (Cadet and Diehl 1984; Wu and Hastenrath 1986) are due to common low-frequency fluctuations or to correlation between high-frequency components of the various series. Cadet (1985) finds the existence of a major periodicity at 40 months from spectral analysis of SST, sea level pressure (SLP), air temperature (AT), and wind time series over different areas of the Indian Ocean. He suggests that this timescale may be associated with the SO. Joseph and Pillai (1984) claim that apart from the annual cycle the only prominent periodicity of Indian Ocean SST is a triennial oscillation, but their results are obtained from a very short record (1961–1973). On the other hand, recent ENSO-related works suggest that variabilities in the Asian monsoon region and Pacific Ocean are mainly correlated at a biennial timescale (Meehl 1987, 1993; Yasunari 1990; Ropelewski et al. 1992). However, biennially filtered SST, SLP, and wind series seem to account for only a small part of the total monthly SST, SLP, and wind variance over the Indian Ocean (Barnett 1991, his Fig. 2; Ropelewski et al. 1992, their Figs. 5 and 7). Moreover, it must be emphasized that ISM rainfall series is not basically biennial as it is assumed by Meehl (1987) or Yasunari (1990), but rather exhibits a triennial oscillation as many monsoon indicators (Bhalme and Jhadav 1984). Thus, the major timescales of climate variability over the Indian Ocean need further investigation both from the points of view of their links to ENSO and to ISM rainfall.

These rather confusing results have led to the current study. We are primarily interested in documenting the low-frequency evolution of the surface fields over the Indian Ocean and in assessing their relationships with the activity of ISM. This may provide some new insights into the mechanisms of interannual variability of the monsoon systems and their links to ENSO.

2. Data sources and methods

Many datasets currently used to assess the variability of the monsoon systems are subjected to important systematic errors (Terray 1994). Thus, a basic step if we want to get new insights into the interannual variability of ISM is to develop new, quality-checked databases. This effort has been documented in Terray (1992). We will just give here a brief summary of the main steps involved in the construction of these datasets.

a. The land dataset

First, monthly time series of SLP (59 stations), AT (73 stations), and rainfall (73 stations) originated from various countries in the Indian monsoon region were extracted from NCAR's World Monthly Surface Station Climatology (WMSSC; Spangler and Jenne 1984). This data collection covers the period 1900–1980 but has been extended here to 1984 with published data in *Monthly Climatic Data for the World* (U.S. Weather Bureau 1981–1984).

Next, all these data have been adjusted to reduce bias effects due to change in observation time for the SLP data or station moves for the AT data (Terray 1994). No corrections have been applied to rainfall data.

After this correction phase, many gaps in the time series have been filled with new data obtained from the *India Weather Review* (Monthly Weather Reports) collection published by the Indian Meteorological Department (IMD) and time series for 61 new rainfall stations, as well as 19 new SLP stations, were added to the dataset to obtain uniform coverage over the Indian subcontinent. All the new SLP data were corrected with the same procedures as outlined in Terray (1994).

Finally, efficient tests for detecting outliers (the Shapiro–Wilks test; Barnett and Lewis 1978) were applied to the resulting 20 592 monthly series, increasing somewhat the number of missing values but eliminating many suspicious values in the time series.

After all the data manipulations, the final networks are 135, 73, 78 stations, while the number of missing values reaches 20%, 15%, and 40% for the rainfall, AT, and SLP parameters, respectively. It should be emphasized that no interpolation techniques have been used to fill in the missing gaps in the monthly time series. Finally, the fields for each parameter have been normalized by the monthly means and standard deviations computed for the 1900–1970 period.

b. The marine dataset

A description of the marine dataset used here may be found in Terray (1994). First, only the SLP, SST, and AT ship reports will be fully examined in this paper because many problems remain to be solved for other parameters. The size of the domain has also been reduced to 6°S–30°N and 30°–100°E because outside these limits the data are so sparse as to be of question-

able value. The data are presented as monthly means in 2° latitude by 2° longitude boxes and the period of analysis extends from 1900 to 1986.

The SST, AT, and SLP ship reports sampled over the Indian Ocean are affected by climatic as well as instrumental discontinuities and trends (Terray 1994). These characteristics of the marine fields cause some problems in defining anomalies in the traditional sense: how can we define the mean state for each parameter in order to assess the short-term interannual variability when time series for most of the grid points are not stationary?

These difficulties have been overcome here by a preliminary correction of the marine fields. The method aims at giving reasonable anomaly fields for interannual studies by detrending and adjusting the marine series for the main discontinuities. In the rest of this section, we will outline this correction procedure of the marine fields.

1) First, all the monthly fields were objectively analyzed with a successive correction method taking climatological means from an atlas as a first-guess field (Cadet and Diehl 1984). This scheme effectively removes most of the systematic errors that are due to the shift of the main shipping routes, as well as spurious values that can be observed along some ship tracks.

2) Next, the simple procedure of subtracting mean values in periods between the main climatic and/or artificial jumps (1940, 1954, 1976) identified in Terray (1994) was used to derive a first estimate of the anomaly fields. That is, the periods 1900–1939, 1940–1953, 1954–1976, and 1977–1986 were treated separately to compute means and anomalies for each parameter.

Changes in observing times seem to explain the spurious jump observed during the 1930s for SLP and AT (Terray 1994). An additional problem affects the SST records during 1900–1939 since it is believed that most of SST ship reports before 1940 were made with uninsulated buckets that are biased low, while the data after the 1940s are mostly insulated bucket or injection measurements that are biased high (Bottomley et al. 1990). The 1954 jump is only evident in SST series, however, SLP and AT anomalies were also computed separately for 1940–1953 and 1954–1976 since this will facilitate comparisons between the various oceanic fields. Finally, the 1976 jump is evident for all the parameters and seems to reflect, at least partly, a real climatic change over the Indian Ocean (Terray 1994).

3) We are now in a better position to overcome the trend problem, but the different trends have to be estimated on each time segment separately in order to take into account the mean's adjustment used to remove the main discontinuities in step 2). This has been done by fitting robust regression models with linear and quadratic time trends as regressors to each of the parameter–gridpoint–segment anomaly series computed in step 2). Dummy variables were also included in the regressions in order to correct some biases observed during short periods (especially, during the two world wars). Only the significant trends have been removed from the anomaly series. A discussion of the origins of these trends may be found in Terray (1994).

4) Finally, the time segments for each parameter have been recombined together to give final estimates of the anomaly fields. These corrected fields have been monthly normalized with standard deviations computed on the whole 1900–1986 period, but without the sample months from the two world wars (1916–1918, 1940–1945).

c. *Methodology*

Traditional (e.g., Kutzbach 1967) and rotated (e.g., Richman 1986; the Varimax method) Empirical Orthogonal Function (EOF) analyses have been used to extract the dominant patterns of interannual variability of the various monthly fields during the 1900–1970 period. For each parameter, the computations have been undertaken separately for the land and marine datasets. In this fashion, we have a simple method to cross validate our results and to compensate for the deficiencies in both sources, for example, the missing problem for the land records and the mixed bias-trend problem for the ship dataset.

The unreliable monthly marine fields of both the 1916–1918 and 1940–1945 periods have not been used actively in the various EOF analyses of the ship dataset. Instead, the time coefficients of these periods have been computed a posteriori by projecting these monthly fields onto the eigenvectors of each analysis. This method appears to be a very simple and convenient way to obtain more robust estimates of our principal and rotated patterns over the ocean since the highly suspicious observations during both world wars can unduly affect the orientation of the eigenvectors in each EOF analysis.

It is not possible to apply directly standard EOF methodology to the land dataset since many missing gaps exist in the various fields. We will now briefly outline how this problem has been handled.

EOF analysis has been derived in a variety of different ways in the meteorological literature, (see, for example, the papers by Kutzbach 1967; Jalickee and Hamilton 1977; or Richman 1986). As noted by Horel (1981), all these derivations of the method can be shown to be equivalent and differ essentially by the terminology used and the way the results of the analysis are presented. However, among these various methods of derivation, the one based on the mathematical concept of the singular value decomposition (SVD) of a matrix (Jalickee and Hamilton 1977) can be directly extended to handle missing values in the data as the others do not.

To demonstrate this, let $\mathbf{X}$ be an $p \times n$ data matrix, with $p \leq n$. Without loss of generality, we will consider

that the lines of $\mathbf{X}$ referred to stations and columns to time observations (e.g., months, seasons, . . .). We assume first that $\mathbf{X}$ does not contain missing cells in order to introduce the SVD mathematical concept. Then, the SVD of $\mathbf{X}$ is

$$\mathbf{X} = \mathbf{U}\Sigma\mathbf{V}^t, \tag{1}$$

where

$$\mathbf{U}^t\mathbf{U} = \mathbf{V}\mathbf{V}^t = \mathbf{I}_p, \quad \Sigma = \begin{pmatrix} \lambda_1, & 0, & & 0 \\ 0, & \lambda_2, & & 0 \\ & & \ddots & \\ 0, & & 0, & \lambda_p \end{pmatrix}$$

and $\mathbf{I}_p$ represents the identity matrix of order p. The numbers $\lambda_1, \lambda_2, \ldots, \lambda_p$ are the nonnegative square roots of the eigenvalues of $\mathbf{X}\mathbf{X}^t$ and are called the singular values of $\mathbf{X}$. It may be assumed that

$$\lambda_1 \geqslant \lambda_2 \geqslant \cdots \geqslant \lambda_p \geqslant 0. \tag{2}$$

Elements $\mathbf{U}_{1k}, \mathbf{U}_{2k}, \ldots, \mathbf{U}_{pk}$ and $\mathbf{V}_{1k}, \mathbf{V}_{2k}, \ldots, \mathbf{V}_{nk}$ form the kth left and right singular vectors of $\mathbf{X}$, respectively. These vectors are the orthonormalized eigenvectors of $\mathbf{X}\mathbf{X}^t$ and $\mathbf{X}^t\mathbf{X}$, respectively. A proof of the SVD can be found in standard books on numerical analysis such as Lawson and Hanson (1974). The links between the SVD of a matrix and the traditional derivation of the EOF method in the meteorological literature (e.g., Kutzbach 1967) may be easily shown. Defining

$$\mathbf{C} = \Sigma\mathbf{V}^t, \tag{3}$$

it follows that

$$\mathbf{C} = \mathbf{U}^t\mathbf{X} \quad \text{and} \quad \mathbf{X} = \mathbf{U}\mathbf{C}.$$

These two relations correspond to (8) and (9) in the approach followed by Kutzbach (1967).

The interest of the SVD for extending the EOF method to the case where $\mathbf{X}$ contains missing values lies in the fact that the first q terms of the SVD of $\mathbf{X}$ form an optimal approximation to the original matrix in the sense of least squares. That is, for any $p \times n$ real matrix $\mathbf{X}$ with representation (1) and any integer $q \leqslant p$, the minimum of

$$\|\mathbf{X} - \mathbf{Y}\|^2 = \sum_{ij} (\mathbf{X}_{ij} - \mathbf{Y}_{ij})^2 = f(\mathbf{Y}) \tag{4}$$

on all $p \times n$ matrix $\mathbf{Y}$ of rank less than or equal to q is obtained if and only if

$$\mathbf{Y} = \hat{\mathbf{X}}^q = \mathbf{U}_q\Sigma_q\mathbf{V}_q^t, \tag{5}$$

where $\mathbf{U}_q$, $\mathbf{V}_q$, and Σ_q stand for submatrices formed by the first q columns of $\mathbf{U}$, the first q columns of $\mathbf{V}$, and the first q lines and q columns of Σ, respectively. Moreover, this minimum is equal to

$$f(\hat{\mathbf{X}}^q) = \sum_{ij} (\mathbf{X}_{ij} - \hat{\mathbf{X}}_{ij}^q)^2 = \sum_{k=q+1}^{p} \lambda_k^2. \tag{6}$$

This result is known as the Eckart–Young theorem (see Lawson and Hanson 1974, 26).

This scheme of successive approximations can be readily extended to estimate a q principal components solution when $\mathbf{X}$ contains some missing values. That is, we can correspondingly seek a minimum of

$$\sum_{ij} (\mathbf{X}_{ij} - \mathbf{Y}_{ij})^2 = f(\mathbf{Y}) \tag{7}$$

on all $p \times n$ matrix $\mathbf{Y}$ of rank less than or equal to q in the incomplete case, but here the summation is restricted over the i, j values such that $\mathbf{X}_{ij}$ is observed. Suppose now that a minimum of $f(\mathbf{Y})$ has been found by a suitable nonlinear minimization algorithm and let $\tilde{\mathbf{X}}^q$ be such a solution. Here $\tilde{\mathbf{X}}^q$ will possess a SVD with no more than q terms with a singular value distinct from zero since $\tilde{\mathbf{X}}^q$ is of rank q. Consequently, the fact that $\tilde{\mathbf{X}}^q$ is a minimizer of $f(\mathbf{Y})$ shows that this SVD of $\tilde{\mathbf{X}}^q$ can be taken as an optimal approximation in the sense of least squares of the first q terms of the true SVD of $\mathbf{X}$ in the incomplete case.

From this approximation of the first q terms of the SVD of $\mathbf{X}$, the first q principal component time series, the eigenvalues or amounts of variance explained by each of these q principal components and the spatial loading vectors associated with them (which are defined in this paper as the product of the eigenvectors of $\mathbf{X}\mathbf{X}^t$ by the square root of their associated eigenvalues when $\mathbf{X}$ is complete) can readily be obtained and analyzed in the traditional manner. The interested reader will find more numerical details on this generalized EOF procedure in the appendix. Procedures for estimating the q parameter (e.g., the number of principal components to be estimated) before the generalized EOF analysis are also summarized in appendix.

Standard spectral analysis (based on a Fast Fourier Transform algorithm) has been applied to the EOF time series for depicting the timescales involved in the interannual variability of the monthly fields. Spectra have been computed not only on the overall 1900–1970 period but also for three subperiods of equal length: January 1900–August 1923, September 1923–April 1947, and May 1947–December 1970, denoted period I, period II, and period III, respectively. The choice of these periods is based on results of Parthasarathy et al. (1987, their Fig. 3): many widespread drought years were observed in India during period I, while many flood years have occurred during period III. Finally, the observed frequency of drought–flood conditions is quite low during period II. Thus, by analyzing separately our three time segments we can obtain some useful information on the amplitude modulations of the timescales that could exist in the time series during distinct monsoon regimes. On each autospectrum, the 95% significance level based on a red or white noise continuum (depending on the significance of the first serial autocorrelation coefficient) has been plotted.

3. Space–time structure of SLP monthly anomalies

The normalized departures SLP fields over the Indian Ocean and subcontinent during 1900–1970 were analyzed according to the EOF methods of section 2. All the calendar months, January to December, were included in the analyses presented in this section.

The eigenvalues of the first ten modes of Indian Ocean SLP EOF analysis expressed as percentages of the total variance are shown in Table 1. According to the rule of thumb given by Overland and Preisendorfer (1982), only the first three modes may be significant. A two-principal-component model was estimated from the incomplete SLP land data by the missing EOF method described in section 2 because the same EOF-filtering rule applied to a correlation matrix estimated from the land dataset suggests that only two modes may be distinguishable from white noise in this case (see the appendix). The estimated amounts of variance explained by these two approximated EOFs are 64% and 11% (see the appendix). Finally, a Varimax rotation has been applied to the first two modes of the land EOF analysis. The computations suggest the existence of two modes of SLP variability in the Indian region.

a. The low-frequency mode of SLP variability

The first EOF of Indian Ocean SLP monthly fields is shown on Fig. 1a. It describes a domain wide pattern of variation and accounts for 44% of the total SLP variance. The power spectrum of the associated principal component shows a prominent spectral peak that extends over a 4–6-yr period during periods I and III (Figs. 2a,c), while the spectrum during period II (Fig. 2b) is not distinguishable from one expected from a red noise process. The spectra computed on the second Varimax component of SLP land series show similar significant spectral peaks at the 4–6-yr periodicity (Figs. 2d,e, f). Inspection of the associated spatial pattern (Fig. 1b) suggests that this timescale is a dominant feature of SLP variability over Peninsular India. This is consistent with the high spatial loadings of oceanic areas surrounding Peninsular India in Fig. 1a.

TABLE 1. Percentage eigenvalues of the first ten modes of Indian Ocean SLP EOF analysis.

Number	Eigenvalues (%)
1	44.0
2	9.6
3	7.1
4	4.2
5	3.4
6	3.1
7	3.0
8	2.8
9	2.5
10	2.0

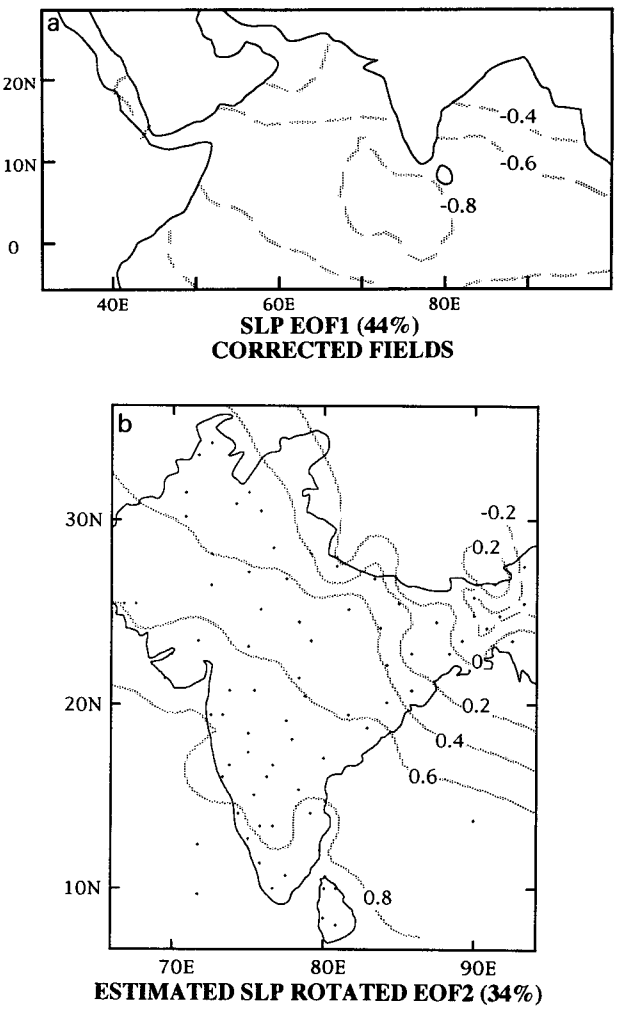

FIG. 1. (a) Spatial pattern of the first EOF of SLP monthly normalized anomaly fields over the Indian Ocean during 1900–1970. See text for details. (b) Spatial pattern of the second Varimax component of SLP monthly normalized anomaly fields on the Indian subcontinent during 1900–1970. The number in parentheses shows a statistical estimate of the percentage of variance accounted for by this mode. See the appendix for details.

Coherence and phase spectra of these SLP principal and Varimax components have been computed (figures not shown). During periods I and III, coherence squares are significant at the 95% level for oscillations with periods ranging from 2 to 10 years, with those among 4 and 6 years having the largest values (0.8 or 0.9). Moreover, the associated phase differences demonstrate that the two series are exactly in phase for these particular frequencies. On the other hand, the coherence squares are very weak at periods of 4–6 years during period II.

There are several possible reasons for this change in the coherence between these two time series during period II. First, this result may be attributed to the overall weakness of the ship data during the 1930s and the

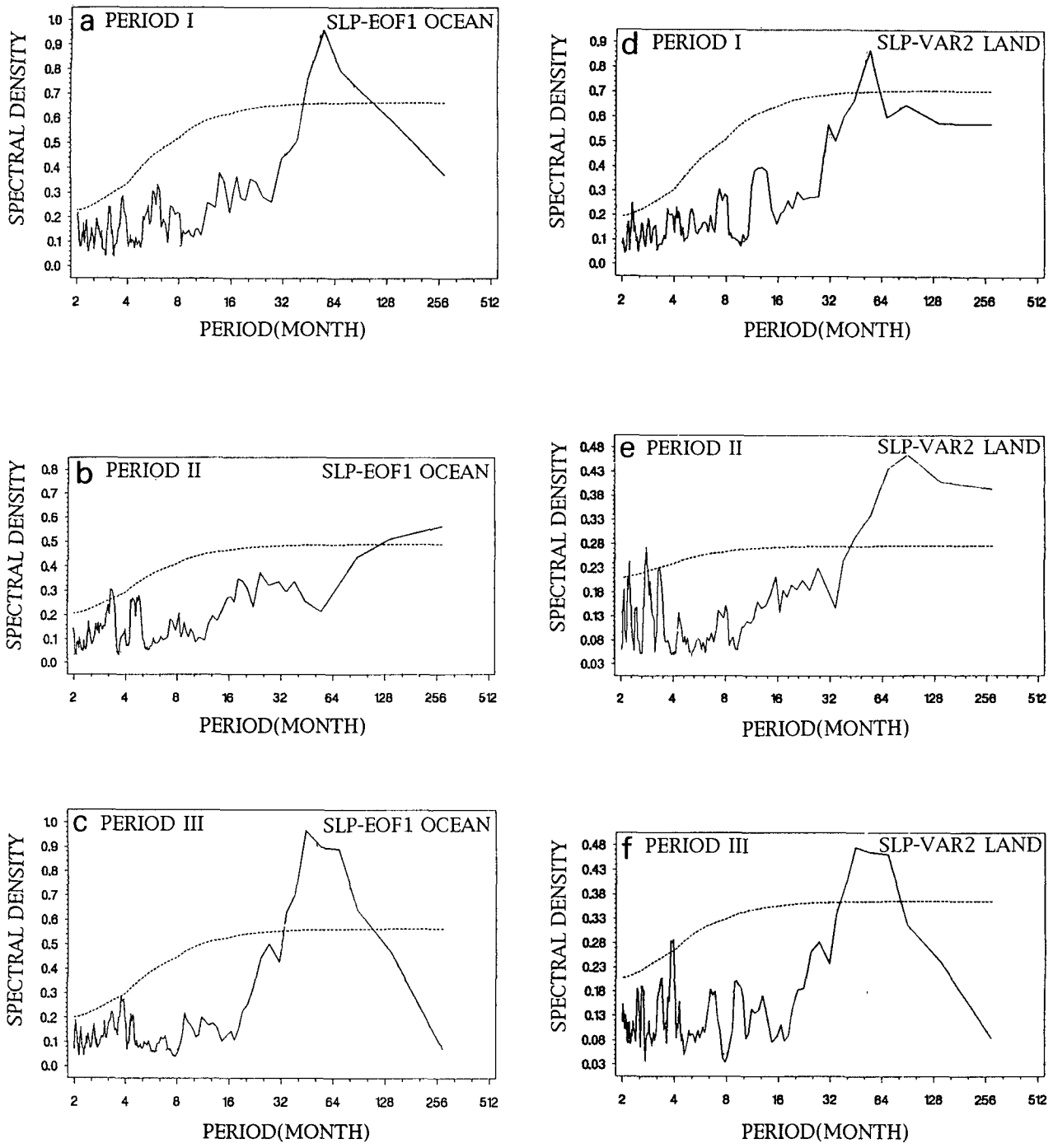

FIG. 2. Power spectrum of EOF1 component of Indian Ocean SLP fields during period I (a), period II (b), and period III (c). Power spectrum of second Varimax component of SLP fields on the Indian subcontinent during period I (d), period II (e), and period III (f). Also shown are red noise 95% confidence levels.

1940s since the 4–6-yr mode is still apparent on the land data during period II (Fig. 2e). However, there are other indications that this decrease in coherence of the low-frequency mode may reflect real changes in the atmosphere. For example, the amount of SLP variance explained by the low-frequency timescale has also largely decreased over the continent from period I to period II (Fig. 2). Moreover, a general decrease in correlation between various atmospheric and oceanic quantities in the Indo-Pacific areas around World War

II has been previously noted by Elliott and Angell (1987, 1988) and Trenberth and Shea (1987), and the weakness of the low-frequency timescale during period II can be linked to such changes in climatic pattern.

As a final note, and without taking into account the results obtained from period II with the ship data, we may remark that the 4–6-yr mode was stronger at the beginning of this century (Figs. 2a,d), while its influence seems to have decrease on the land during recent decades (Fig. 2f).

b. The biennial mode of SLP variability

The second EOF of Indian Ocean SLP fields and the first Varimax pattern of SLP land data are shown in Fig. 3. Both of these loading vectors describe a southwest–northeast anomaly gradient in the SLP fields. The associated principal and Varimax components account for 10% and 40% of the total SLP variance for the ship and land data, respectively (recall that in the case of the land data this percentage is only an estimate, see the appendix).

The only consistent low-frequency timescale on these time series is the biennial periodicity (Fig. 4). Thus, it seems that biennial variability is mainly associated to a southwest–northeast SLP anomaly gradient in the Indian areas. This agrees with a result of Barnett (1991, his Fig. 2), which suggests that biennial SLP variability in the Indian areas (north of the equator) is mainly confined to the Bay of Bengal and over North India and in the western equatorial region near the African coast. However, Fig. 3 completes this result by suggesting that SLP fluctuations over these two areas are negatively correlated at the biennial timescale.

In order to confirm this hypothesis, a cross-spectral analysis has been undertaken on the corresponding amplitude time functions on each time segment (figures not shown). The coherence square between the two series is high and significant for oscillations with periods of two years during period II and marginally significant during period I. In addition, the associated phase differences demonstrate that the biennial modes over the continent and the ocean are exactly in phase. This confirms the inverse relationship suggested above, at least during periods I and II.

Also worth noting in Fig. 4 is that the amplitude of biennial variability decreases regularly on the land from one subperiod to the next, whereas its variance increases steadily over the ocean throughout the record. During period I, the biennial peak exists but is not significant over the ocean, while it is well-defined and very close to the 95% confidence level on the land. During period II, the biennial peak becomes significant at the 90% level for the ship data, whereas the magnitude of the biennial peak has decreased in the land data even if this peak is now significant at the 95% level. Finally, during period III, the biennial oscillation is significant at the 95% confidence level for the ship data, while it has totally disappeared from the land analysis.

The space and time patterns of SLP anomalies associated with low-frequency and biennial oscillations seem quite distinct across the Indian Ocean. It is worth noting that many drought years were observed in period I when the low-frequency mode was dominant, while flood years were more frequent in period III when the biennial mode is particularly well-defined (Parthasarathy et al. 1987). All these results suggest that these two modes can be thought as separate entities or, at least, are derived from different forcing mechanisms. Hereafter, we will refer to these two modes as the B and LF modes of monsoon variability, respectively.

4. Low-frequency oscillations and the intensity of the Indian Summer Monsoon

In this section, the main emphasis will be on determining the contribution of the LF and B modes of atmospheric variability in the spatial and temporal evolution of ISM.

All the eigenvector analyses presented in this section have been computed from monthly standardized series of the calendar months from June to September only. Three components were retained in the analyses of the SLP fields over the Indian Ocean and subcontinent, while only two components were extracted from the rainfall monthly series by application of EOF filtering rules. These various principal component models were then subjected to a Varimax rotation.

In the following discussion, the notations R1 and R2 (respectively, P1, P2, and P3 for SLP fields) are used to denote rainfall Varimax spatial patterns, while the corresponding lower case symbols, r1 and r2 (respectively, p1, p2, and p3 for SLP fields), denote the corresponding Varimax components series.

a. Space and time scales of rainfall and SLP anomalies during ISM

The two Varimax spatial patterns (R1 and R2) of summer monthly rainfall anomalies for 135 stations over the whole Indian subcontinent during the 1900–1970 period are shown in Fig. 5. The estimated amounts of variance explained by r1 and r2 are 13% and 9%, respectively. These estimates of the fractions of rainfall variance described by r1 and r2 are quite low, showing that the rainfall anomaly fields contain considerable amounts of small-scale noise during ISM. Broad-scale rainfall anomaly patterns are nevertheless apparent in Fig. 5.

Interannual rainfall fluctuations over the western Ghats and in the Indo-Gangetic plains are in the same phase on Fig. 5a. Since the rainfall in the Gangetic plains is to a large extent associated with the frequency and strength of traveling monsoon depressions coming from the Bay of Bengal, this result suggests that the

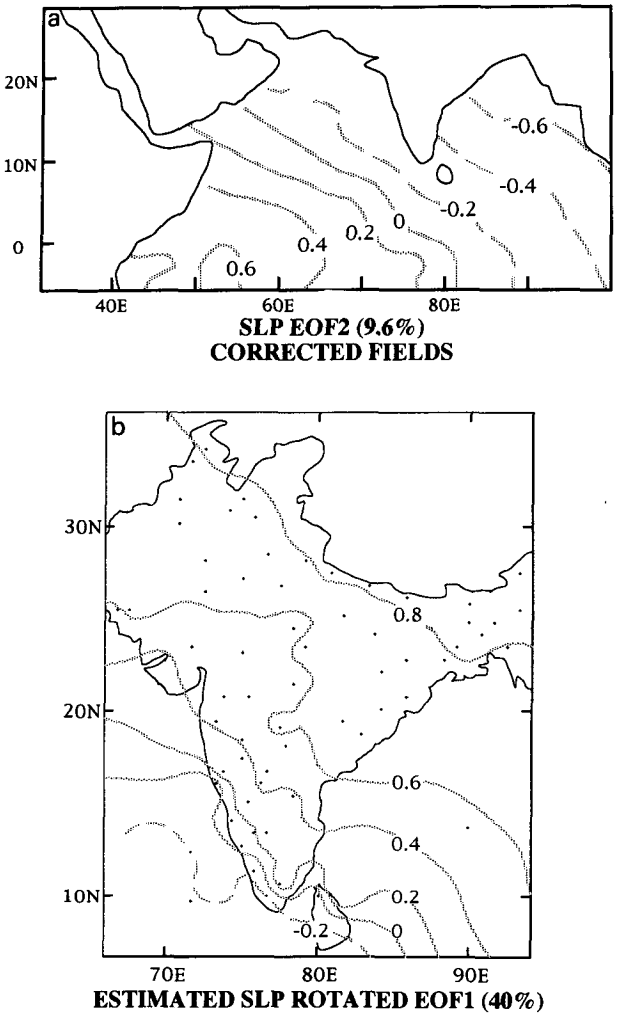

FIG. 3. (a) Spatial pattern of the second EOF of SLP monthly normalized anomaly fields over the Indian Ocean during 1900–1970. (b) Spatial pattern of the first Varimax component of SLP monthly normalized anomaly fields on the Indian subcontinent during 1900–1970.

number and/or intensity of these disturbances are also well correlated to the strength of the monsoon flow that determines the intensity of the orographic rains over the west coast. Rainfall fluctuations in the northeastern part of the Indian subcontinent are more or less out of phase with rainfall variations in the two preceding areas. This agrees with the case study of the 1987 ISM by Krishnamurti et al. (1989) or composite analysis of rainfall anomalies during drought or flood years by Bhalme and Mooley (1980). Both papers emphasized that heavy rainfall is observed along and near the foot of Himalayas when most parts of the Indian subcontinent have deficient rainfall.

Rainfall variations over Peninsular India are largely described by R2 (Fig. 5b). Some out-of-phase relationship between Peninsular India and stations in the northeast part of the Indian subcontinent can also be detected on R2 as for R1, but this southwest–northeast contrast is somewhat shifted to the southwest on R2. Thus, this shift of the rainfall contrast over the land may be associated with a more southerly position of the monsoon trough, which is generally favorable for an active monsoon (Bhalme and Mooley 1980; Shukla 1987).

The results of the Varimax analysis on SLP land data are shown on Figs. 5c, 5d, and 5e. The estimated fractions of total SLP variance described by p1, p2, and p3 are 34%, 23%, and 20%, respectively. This shows the broad-scale nature of SLP fields during ISM.

Here P1 contains high spatial loadings over the northern part of Indian subcontinent (Fig. 5c), thereby representing an excess or deficit of mass over this area. The largest anomalies are found in central parts of India on P2 (Fig. 5d). Thus, p2 may be associated with amplitude fluctuations of the monsoon trough that lies normally over the Gangetic plains (Bhalme and Mooley 1980). Finally, high spatial loadings on P3 are mainly concentrated in Peninsular India (Fig. 5e).

In order to show that large fluctuations in ISM rainfall are linked to broad-scale SLP anomaly patterns, Table 2 gives monthly cross correlations between concurrent values of SLP and rainfall Varimax components. For assessing the significance of these cross correlations, we recall that the 99% and 95% confidence limits for a sample size of 71 (years) are 0.3 and 0.24, respectively. These confidence limits are entirely valid here because none of the June, July, August, and September subseries extracted from the SLP and rainfall Varimax components have a lag 1 autocorrelation significant at the 95% level.

Table 2 shows a highly significant relationship between r1 and p2. This association suggests that p2 can be taken as an index of the deepness of the monsoon trough over the Gangetic plains. Also worth noting is that this rainfall–SLP relationship steadily increased from June to September since the cross correlations between r1 and p2 rise progressively from −0.7 to −0.89.

During the most active monsoon months, July and August, highly significant associations are also observed between r2 and p1 and p3. This agrees with the hypothesis that r2 is associated with the latitudinal shift of the main axis of the monsoon trough during ISM. A more southerly (northerly) position of the monsoon trough is associated with positive (negative) rainfall anomalies over Peninsula and negative (positive) anomalies over Bangladesh and the northeastern part of India.

Finally, we note that correlations between r1 and both p1 and p3, are low and insignificant during nearly all the months. Moreover, the cross correlations between r2 and p2 follow exactly the same pattern. Thus, the two broad-scale patterns of ISM rainfall anomalies are associated to independent modes of SLP variations.

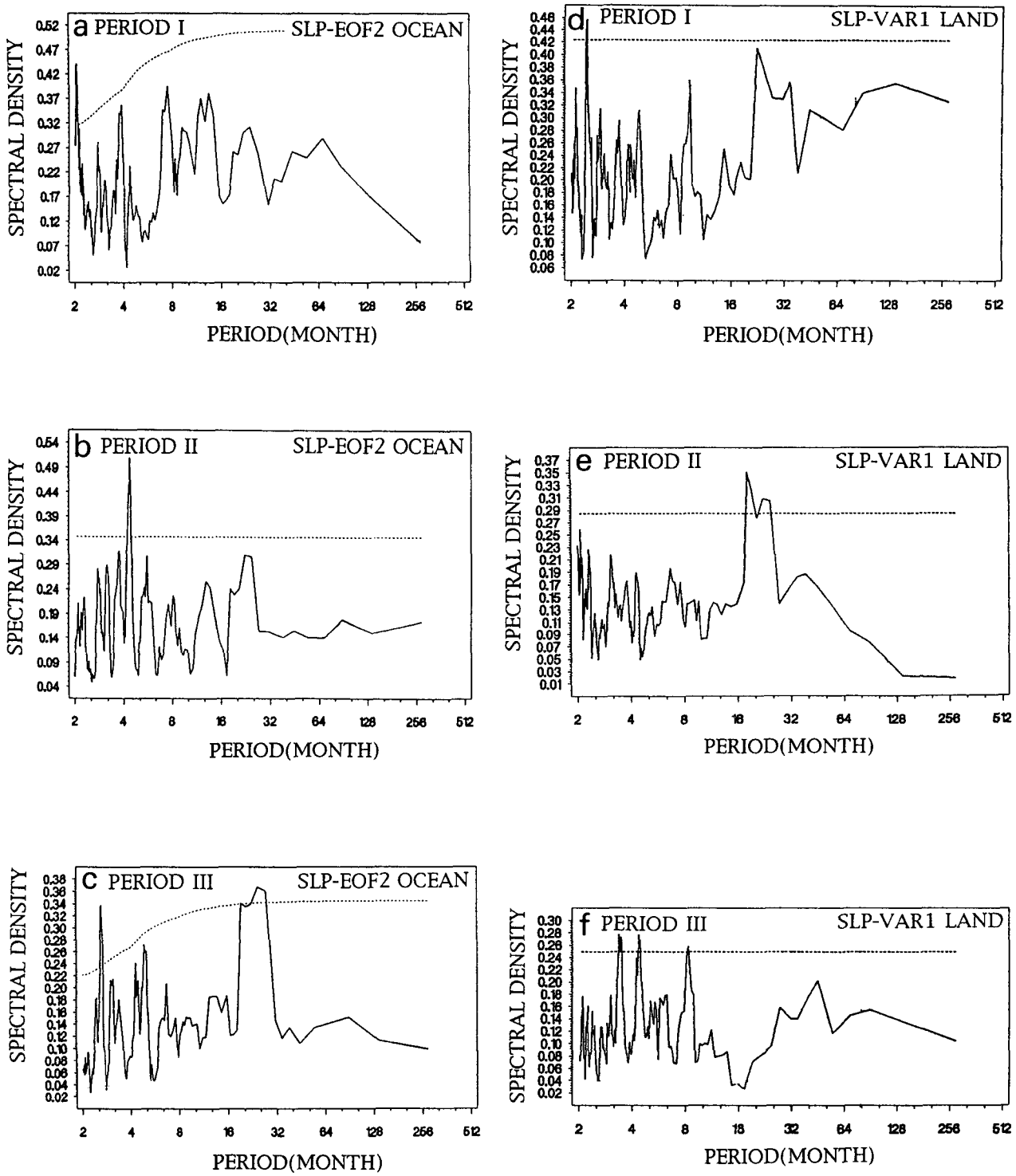

FIG. 4. Power spectrum of EOF2 component of Indian Ocean SLP fields during period I (a), period II (b), and period III (c). Power spectrum of first Varimax component of SLP fields on the Indian subcontinent during period I (d), period II (e), and period III (f). Also shown are red or white noise 95% confidence levels.

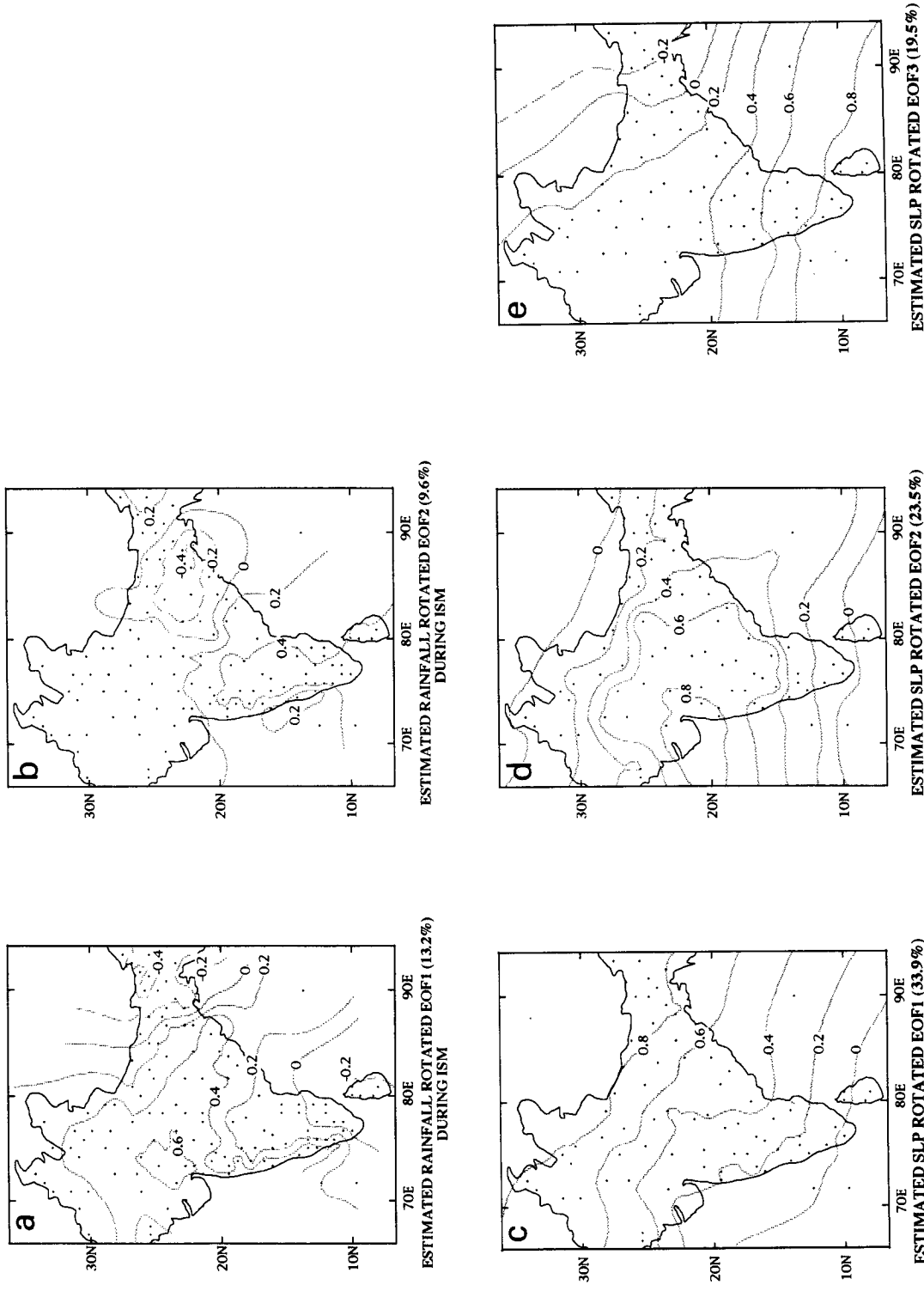

FIG. 5. (a) Spatial pattern of the first Varimax component of rainfall monthly normalized anomaly fields during ISM (6–9). (b) Same as in (a) but for the second Varimax component. (c) Spatial pattern of the first Varimax component of SLP monthly normalized anomaly fields during ISM. (d) Same as in (c) but for the second Varimax component. (e) Same as in (c) but for the third Varimax component. The numbers in parentheses show statistical estimates of the percentage of variance accounted for by these modes. See the appendix for details.

TABLE 2. Cross correlations between the Varimax components of rainfall (r1, r2) and SLP (p1, p2, p3) fields during ISM. Cross correlations are given for each month of ISM. Months are identified by 6 = June, 7 = July, 8 = August, 9 = September.

	Month	p1	p2	p3
r1	6	0.46	−0.70	−0.07
r1	7	0.13	−0.80	0.13
r1	8	0.14	−0.86	0.15
r1	9	−0.23	−0.89	−0.15
r2	6	0.37	0.02	−0.19
r2	7	0.52	−0.01	−0.50
r2	8	0.55	0.07	−0.57
r2	9	0.35	−0.12	−0.54

The Varimax analysis of Indian Ocean SLP fields confirms all the above findings (figures not shown). In particular, SLP variations over the central parts of both the Arabian Sea and the Bay of Bengal, which correspond to the mean location of the monsoon trough over the ocean, are significantly associated with r1 and p2, while r2, p1, and p3 are significantly correlated with a southwest–northeast SLP anomaly gradient over the Indian Ocean. This anomaly gradient is similar to the one associated with the B SLP mode (Fig. 3a) and seems to be associated to a shift of the monsoon trough south and west of its normal position. Prasad and Singh (1988) have obtained exactly the same results on the short 1961–1968 period. All these facts confirm again the broad-scale nature of SLP variations associated with ISM rainfall fluctuations.

Finally, we wish to contrast the above results with those of Weare (1979), who found no significant relationships between SLP and rainfall EOFs over the Indian subcontinent during 1949–1972. These discrepancies are mainly linked to the fact that the SLP data used by Weare (1979) are not corrected for artificial biases and to the use of a Varimax rotation in this paper instead of standard EOFs in Weare's study.

b. Contribution of the LF and B SLP modes in the anomaly patterns during ISM

If the B and LF SLP modes exist during ISM, both modes may have a strong impact on ISM rainfall spatial distribution since each of them suggests a modulation of the monsoon activity over India and neighboring oceanic areas.

As an example, the B SLP dipole pattern suggests a southwestward extension or a reduction of the spatial scale of the convective center during ISM, and such translations of the monsoon trough are strongly linked with one of the broadscale patterns of rainfall anomalies over India as noted above. Similarly, the SLP spatial pattern associated with the LF mode suggests a global deepness–weakness of the monsoon trough that must also affect ISM rainfall distribution, particularly over the western Ghats and in the Gangetic plains as described in the preceding paragraph.

In order to show the existence of the LF and B modes of atmospheric variability during ISM, the monthly subseries of r1, r2, p1, p2, and p3, discussed above, were subjected to power spectral analysis. Since none of the lag 1 autocorrelations of the June, July, August, and September series extracted from r1, r2, p1, p2, or p3 is significant at the 95% level, the peaks in all the spectra are tested for significance against a white noise continuum. Many of the spectra for the months of August and September show significant peaks corresponding to the LF and B timescales (figures not shown).

The existence of the B and LF modes during August and September implies that both time and space scales of climatic anomalies may increase during ISM. The higher cross correlations observed between r1–p2, r2–p1, and r2–p3 during July, August, and September compared to those observed in June (Table 2) corroborate this hypothesis. This regular increase of amplitude and spatial extension of climatic anomalies from June to September is also seen in Table 3, which shows the true fractions of the total SLP and rainfall variance described by the missing EOF (or Varimax) models (e.g., p1, p2, p3 and r1, r2) in each month of ISM. These fractions have been calculated by summing (A10) in the appendix separately for each of the 71 June, July, August, and September fields included in the missing EOF analyses. The steady increase of the data compression into the EOF models from June to September is apparent on both the SLP and rainfall analyses, thereby suggesting again the broad-scale nature of the climatic anomalies during the second half of ISM.

In order to confirm this result in another way, four monthly rainfall indices have been computed, one for each month of ISM, by simply averaging the normalized monthly anomalies of our 135 rainfall stations over the Indian subcontinent. These four indices have been correlated with each other and with a global ISM rainfall index (taken from Parthasarathy et al. 1987) on the 1900–1984 period (Table 4). It is noteworthy that correlations between the global ISM index and the monthly indices increase from 0.36 in June to 0.64 in September. Moreover, correlations between succeeding monthly rainfall indices also increase at the end of

TABLE 3. Fractions of monthly variance (%) described by the first two rainfall and three SLP principal components of the ISM monthly fields over the land. Months are identified by 6 = June, 7 = July, 8 = August, 9 = September.

Month/analysis	Rainfall (r1, r2)	SLP (p1, p2, p3)
6	18.2	75.6
7	20.2	79.8
8	25.2	82.6
9	23.8	84

TABLE 4. Correlation coefficients among seasonal rainfall index (ISM) and four monthly rainfall indices during ISM (June, July, August, September). The coefficients exceeding the 1%, 1‰, and 1‰‰ probability level are followed by one star (*), two stars (**), and three stars (***), respectively.

	ISM	June	July	August	September
ISM	1				
June	0.36**	1			
July	0.55***	−0.11	1		
August	0.64***	0.01	0.14	1	
September	0.64***	−0.05	0.32*	0.36**	1

the monsoon and become highly significant between August and September. These new results stress again the regular increase of amplitude and spatial extension of the climatic anomalies during ISM, as suggested above.

All together, these results suggest that the triennial oscillation that is characteristic of various ISM rainfall indices (Parthasarathy and Mooley 1978; Bhalme and Mooley 1980) is due to the distinct spatial influence of the LF and B modes as anticipated by Bhalme and Jadhav (1984). These results also show that the long-range forecasting skill of ISM rainfall anomalies may be associated with amplitude fluctuations of the low-frequency modes described here.

5. Space–time structure of SST monthly anomalies

Almost all the studies that have addressed air–sea interactions over the Indian Ocean, stress the passive role of the ocean in these relationships (Cadet and Diehl 1984; Joseph and Pillai 1984, 1986). It is now important to reexamine this aspect of SST variations in light of the two low-frequency atmospheric modes documented in the preceding section.

a. Timescales of SST variations

We show first the results of an Indian Ocean SST EOF analysis during 1900–1970 in order to assess the space–time structure of SST fields. The percentages of variance explained by the first ten modes are given in Table 5. Only the first three modes are significant according to Overland and Preisendorfer's rule. Nonetheless, we will present only the first mode because the second and third eigenvalues of the EOF analysis are so close that the spatial patterns of the associated modes may be strongly affected by each other.

This function accounts for 30% of the total variance and depicts a coherent and global change over the Indian Ocean, but the main anomaly center is localized near the southern tip of India (Fig. 6a). The first EOF of the AT fields is similar in all respects (figure not shown). Thus, these EOFs can be taken as objectively determined indices of the global SST and AT fluctuations over the Indian Ocean.

The power spectrum of the first SST EOF during the whole 1900–1970 period (Fig. 6b) is not very different from one obtained from a red noise process. However, spectral density coordinates corresponding to the B (or quasibiennial) and LF periodicities are both above the 95% confidence level. This suggests that the B and LF modes may manifest themselves in the SST anomaly fields over the Indian Ocean. Inspection of spectra computed on periods II and III confirms this suggestion since more separate peaks corresponding to the B and LF modes are apparent during these shorter time intervals (figures not shown). During period I, only the LF peak is present, but this peak does not exceed the 95% confidence limit. Finally, it may be noted that spectra calculated on periods I, III, and the whole 1900–1970 interval contain substantial very low-frequency (persistence) energy (Fig. 6b). All these results are also observed on spectra computed on the first AT EOF.

b. SST and SLP relationships at the B and LF timescales

The significance of the ocean–atmosphere interactions at the LF and B timescales may be tested with a cross-spectral analysis between the first SST mode and the various SLP functions presented in section 3. The results of these analyses suggest that the ocean–atmosphere interactions are generally stronger at the B timescale than at the LF frequencies.

The significance of the SLP–SST relationships at the B timescale may be illustrated with the coherence squares and phase differences between the first SST EOF and the second Indian Ocean SLP EOF (Fig. 7), which is closely associated with the B atmospheric mode over the Indian Ocean (see section 3).

No significant B coherences exist between these two series during periods I and II (figures not shown), but coherence squares between these variables are high and significant at the 95% level for oscillations with period ranging from 22 to 26 months during period III (Fig. 7a).

In order to assess the lead or lag relationships between the variables, we recall that the time lead or lag,

TABLE 5. Percentage eigenvalues of the first ten modes of Indian Ocean SST EOF analysis.

Number	Eigenvalues (%)
1	30.0
2	9.1
3	8.6
4	6.2
5	4.4
6	4.2
7	3.7
8	3.2
9	2.1
10	2.0

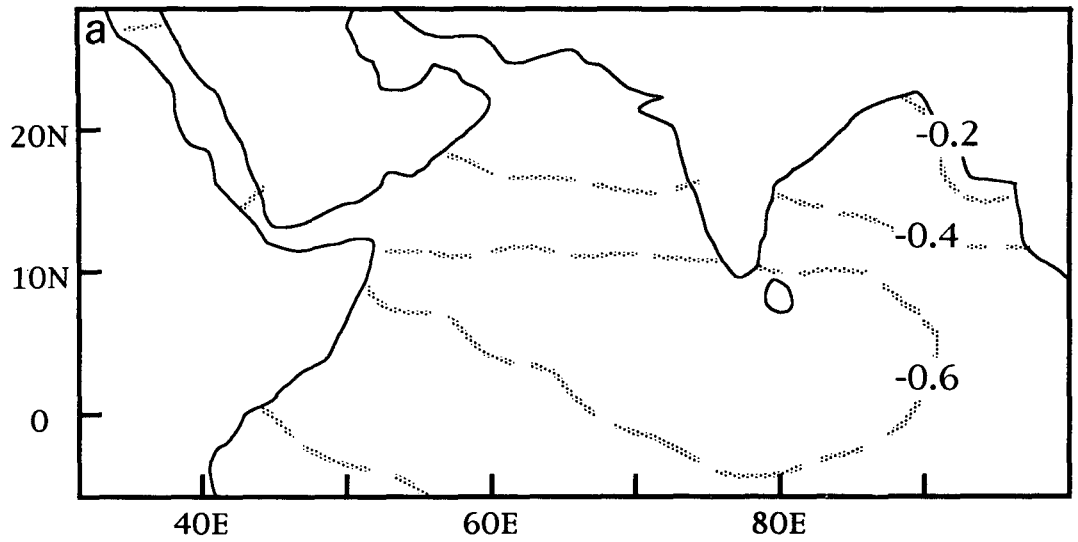

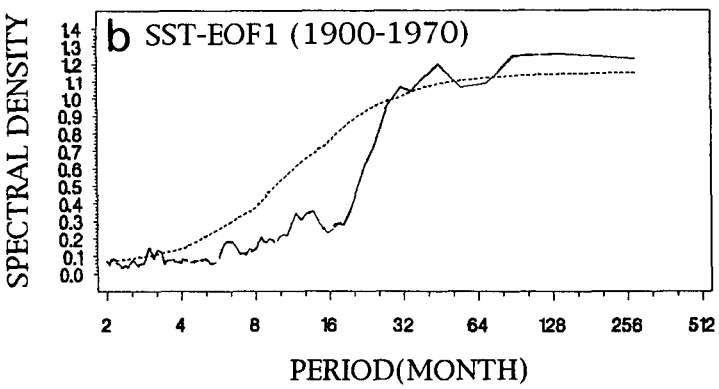

FIG. 6. (a) Spatial pattern of the first EOF of SST monthly normalized anomaly fields over the Indian Ocean during 1900–1970. (b) Power spectrum of SST EOF1 component during 1900–1970. Also shown is red noise 95% confidence level.

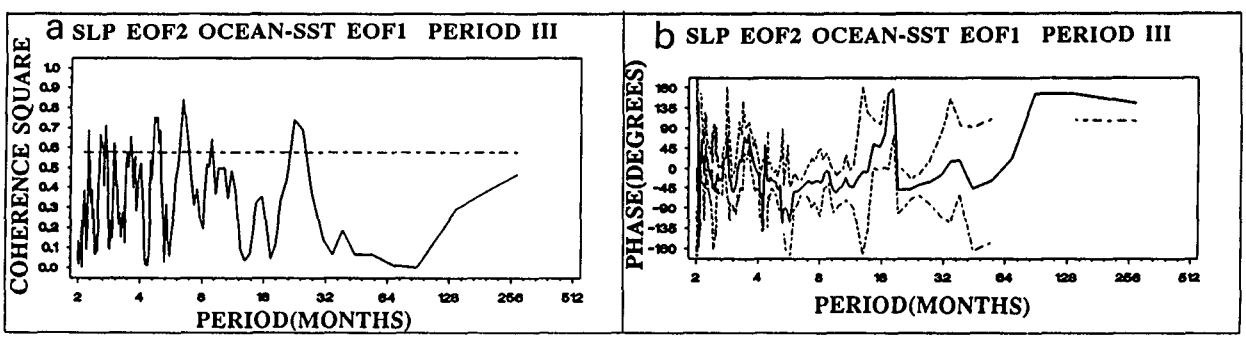

FIG. 7. Cross-spectrum analysis of SST EOF1 and SLP EOF2 components over the Indian Ocean during period III. (a) Coherence square spectrum, 95% level of significance is indicated. (b) Phase differences (degrees), the SLP time series leads for negative values of phase, also included is 95% confidence interval (dashed lines).

say T, of one variable over the other for each frequency component can be derived from the phase spectrum by using the formula $T = (\text{phase} \times \text{period})/360$, where it is understood that the phase is in degrees and the period is in months. Since negative phase corresponds to a time lead of the second SLP EOF on the first SST EOF, phase differences given on Fig. 7b suggest that the atmosphere leads the ocean by about 2 or 3 months at the B timescale during period III.

Cross-spectral analysis between the first SST EOF and the first Varimax component of SLP land data, which is closely associated with the B atmospheric mode on the land (see section 3), also shows a significant coherence between SLP anomalies and SST variations at the B timescale during periods I and II, but no B coherence is found between these two series during period III, when the B atmospheric mode is weaker on the land (figures not shown).

6. Composite analysis of SST, SLP, AT, and rainfall anomaly fields

The preceding section suggests that SST and SLP anomalies over the Indian Ocean are closely related at the B timescale. However, this does not explain the mechanisms of B variability over the Indian Ocean. Therefore, we present now a composite analysis of SLP, SST, AT, and rainfall monthly normalized anomaly fields over the Indian Ocean and subcontinent in order to highlight the space–time evolution of the B mode.

The anomaly fields have been composited for period of two years with respect to drought and flood monsoon years separately. The drought and flood years included in the analysis are 1905, 1911, 1920, 1951, 1965, 1966, 1972, 1974, 1979 and 1933, 1936, 1938, 1956, 1959, 1961, 1975, 1983 respectively. These are the years with the most widespread drought–flood conditions over India during 1900–1984 (Bhalme and Mooley 1980; Parthasarathy et al. 1987; the years 1916–1918 and 1941–1942, which were also largely abnormal, have not been included in the composites because of the bad quality of the marine fields during the two world wars).

The widespread nature of rainfall anomalies during these heavy and deficient rainfall years can be assessed through the rainfall composite maps given on Fig. 8. These composite maps were prepared from ISM rainfall series of the 29 Indian subdivisions tabulated by Parthasarathy et al. (1987). It is also seen in Fig. 8 that these years with heavy or deficient rainfall over most of the subcontinent are accompanied by anomalies of the opposite sign for the northeastern part of India. Thus, this striking feature seems characteristic of both the drought and flood years as well of the two broad-scale patterns of rainfall anomalies (see section 4). Interestingly, the years following the drought years are relatively wet, while the years following the flood years are relatively dry (Fig. 8). Furthermore, the striking increase (decrease) of rainfall in the northeastern part of India when most of the other areas experienced relatively dry (wet) conditions is also apparent during these succeeding years. Therefore, the composite maps suggest a B tendency in ISM rainfall, even if the ISM rainfall series are not basically biennial but rather exhibit a triennial oscillation and if the B timescale is not the dominant atmospheric periodicity in the Indian areas.

SLP, SST, and AT departure fields during drought and flood years and the years following them were then examined in an attempt to explain this B behavior in ISM rainfall. The AT anomaly fields over the Indian subcontinent have been included in the analysis to get a global picture of thermal conditions and land–sea contrasts. These AT composites are plotted on the same maps than the SST composites. The SLP composites for the Indian Ocean and subcontinent are also presented together on the maps. The composites start in the month of January of the drought and flood years.

Weak negative (positive) SST anomalies are observed over the Indian Ocean during the winter months preceding the bad (good) ISMs (figures not shown). The negative SST anomalies strengthen considerably during April and May of the drought years, while the weak positive SST anomalies observed during the flood years have totally disappeared in April and are replaced by strong negative SST anomalies in May. Thus, the SST anomaly patterns just before or at the onset of the monsoon are very similar for the drought and flood years. In light of these results, it is difficult to speculate a relationship between premonsoon months SST anomalies over the Arabian Sea and the heavy or deficient rainfall years considered here.

However, the SLP, AT, and rainfall composite charts for May suggest that the nature of the observed cold SST anomalies is rather different for the heavy and deficient rainfall years since the negative SST anomalies observed during the flood years are associated with strong negative SLP anomalies over the Arabian Sea and enhanced rainfall over the west coast of India, while the reversed is true for the drought years. This suggests that the southwest monsoon starts earlier during the flood years, and this can afford an explanation for the cold SST observed over the Arabian Sea since the onset is followed by a rapid cooling of nearly 2° or 3°C within a short period of several days.

During ISM, the striking feature brought out by the SST composites is the existence of strong SST anomaly gradient for both the deficient and heavy rainfall years. During the drought years, the SST anomaly dipole is first detectable in June, with a positive pole at the western boundary and a negative pole in the central equatorial Indian Ocean. From July to September, the dipole pattern strengthens progressively and slowly moves eastward until positive anomalies cover essentially the entire Arabian Sea (Fig. 9). A broadly reversed SST

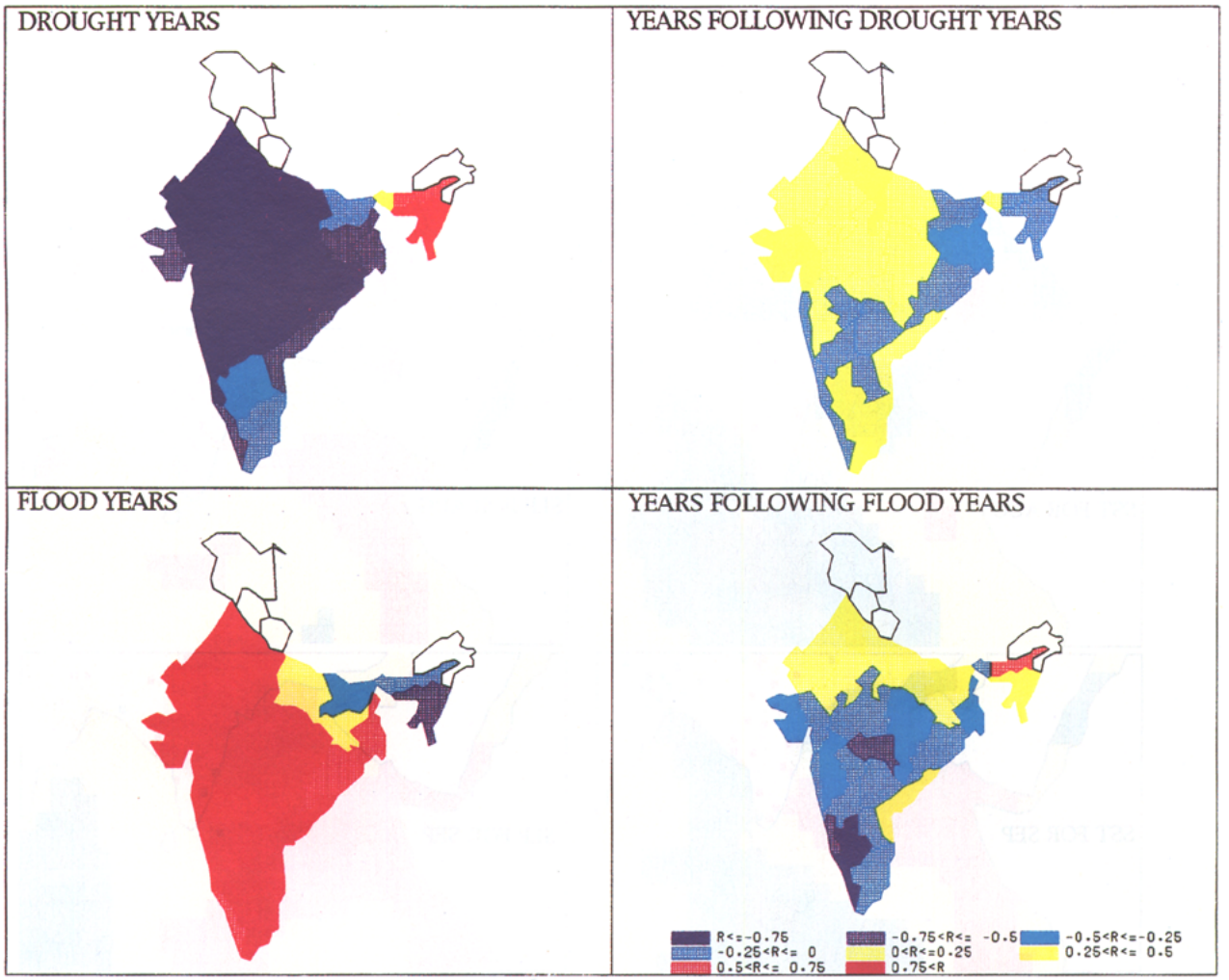

FIG. 8. Composite maps of normalized seasonal rainfall anomaly for 29 meteorological subdivisions over India during eight heavy and nine deficient rainfall years and the years following them. The drought and flood years included in the composites were choosen from the tabulations of Bhalme and Mooley (1980) and Parthasarathy et al. (1987).

pattern is observed during the flood years, but cold SST anomalies appear along the east coast of Africa only from August and then start to propagate eastward during September (Fig. 10).

There is also a regular space–time evolution of SLP anomalies during the dry and wet ISMs (Figs. 9 and 10). First, the broad-scale SLP anomaly patterns observed in July and August suggest that the monsoon trough shifts to a more southwestward position during the flood years as in active monsoon conditions, while the reverse is true for the drought years. This is consistent with the spatial redistribution of rainfall observed during heavy and deficient rainfall years (Fig. 8), as well with the associated AT pattern over the subcontinent.

The SLP composites also suggest the existence of the southwest–northeast SLP anomaly dipole that is associated with the B timescale during ISM of both the deficient and heavy rainfall years. There is a gradual southeastward displacement of the northeast pole of this SLP anomaly gradient that accompanied the eastward propagation of the SST anomaly dipole pattern for both the heavy and deficient rainfall years. On the other hand, the convergence anomalies seem to feedback positively on the SST dipole during both the deficient and heavy rainfall years because the SST gradient strengthens significantly from June to September of these years, as noted above.

Superposed on this SLP anomaly gradient, negative SLP anomalies are first detectable in July of the heavy rainfall years over the peninsula and the surrounding oceanic areas. These negative SLP anomalies progressively grow and expand to cover the entire domain in September of the heavy rainfall years. Such regular

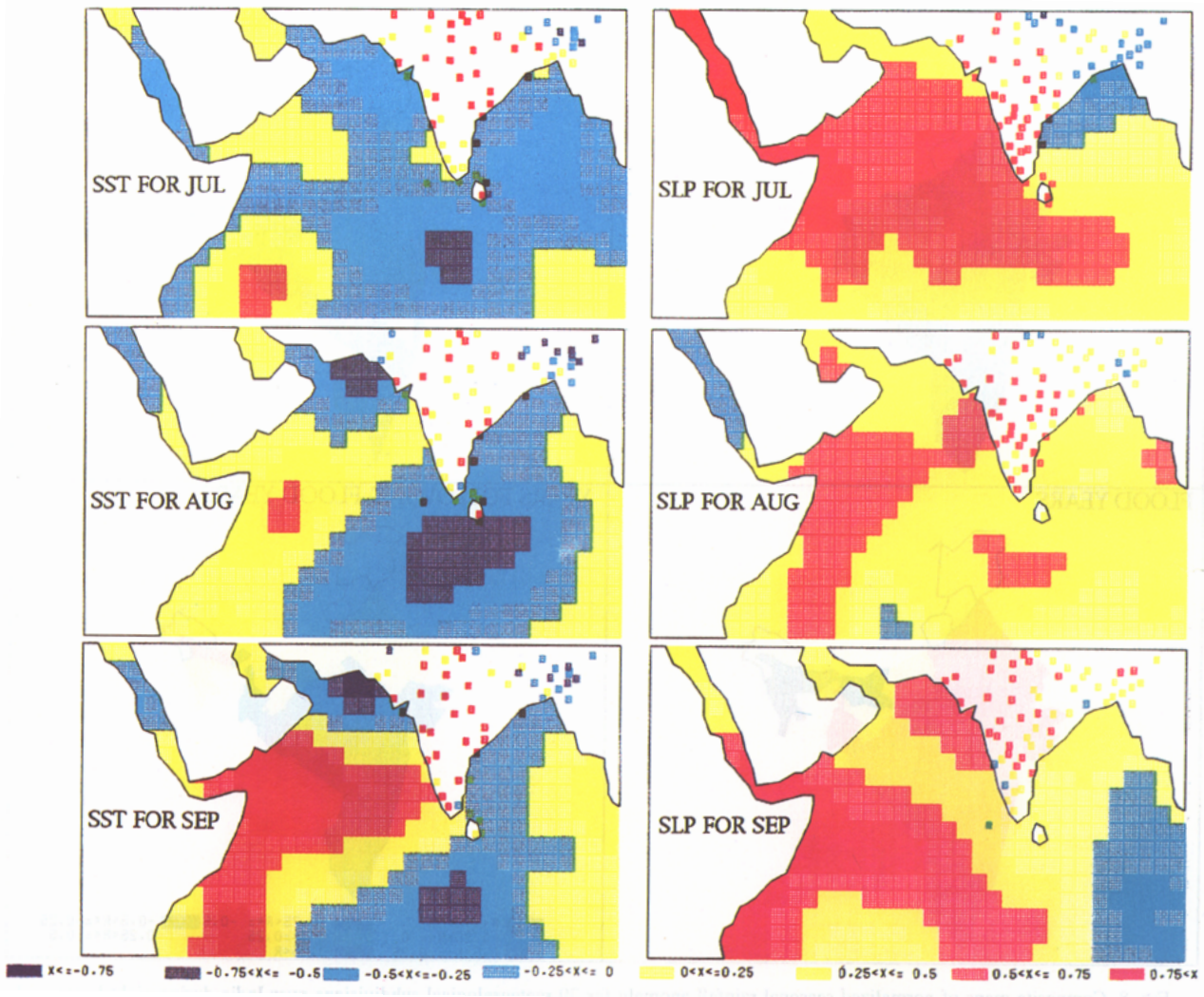

FIG. 9. SST, AT, and SLP monthly normalized anomaly composites for July, August, and September of nine deficient rainfall years.

evolution of the broad-scale SLP anomaly pattern is not apparent for the deficient rainfall years.

During the following winter months, the most prominent features are that the negative (positive) SST and AT anomalies set up at the end of the good (bad) ISMs do not diminish in magnitude (Fig. 11). Surprisingly, the SLP anomalies composites after October (figures not shown) are not well-defined and do not suggest any significant fluctuations of the winter circulation after the heavy or deficient rainfall years, even if the AT anomalies on the land persist month after month.

We see now that premonsoon SST and AT anomalies for the years following the flood (drought) years are strongly negative (positive) over both the Indian Ocean and Indian subcontinent (Fig. 11). The thermal conditions in April, May, and June following the drought and flood years are therefore adverse for the establishment of the next ISM. This point is further supported by the SLP composite charts since weak positive (negative) anomalies cover most of the domain in April, May, and June of the years following the flood (drought) years (figures not shown).

In fact, this symmetric pattern evolution is also observed during the next ISM with below (above) normal SST progressively replacing the warm (cold) anomalies of the spring and late winter succeeding to the deficient (heavy) rainfall years (Figs. 12 and 13). Negative SST anomalies develop by July and spread eastward by August, whereas positive anomalies persist more or less over the eastern part of the Indian Ocean during the whole ISM for the years succeeding to deficient rainfall years. The space–time evolution of the SST anomaly pattern is somewhat more confused during ISM of the years following the flood years since the negative anomalies decay rapidly after June and are replaced by weak positive anomalies in August.

The associated SLP composite maps suggest that the SLP anomalies are partly forced by the SST anomalies.

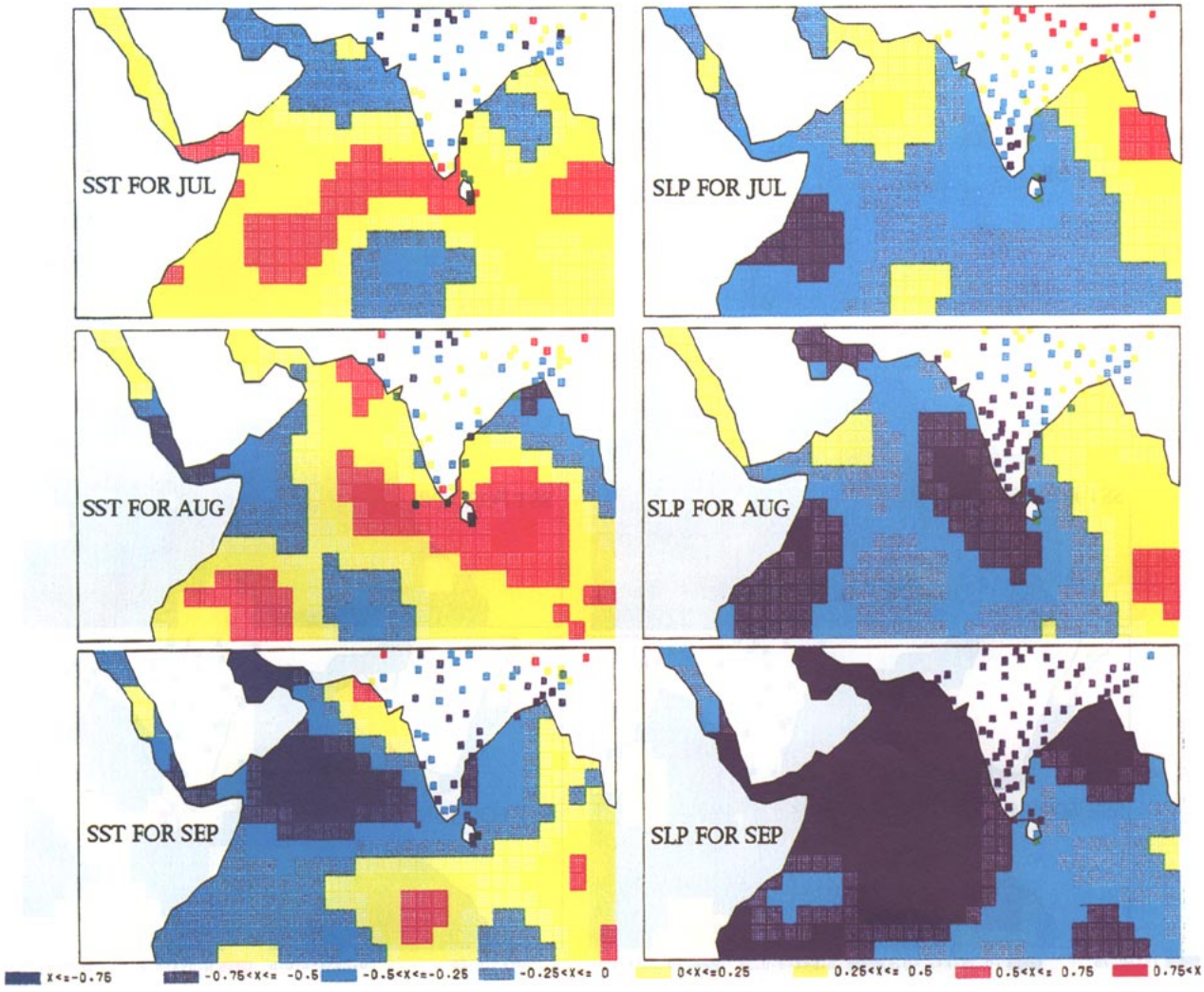

FIG. 10. Same as in Fig. 9, but for eight heavy rainfall years.

Positive SLP anomalies cover most of the domain from June to September of the years following the heavy rainfall years (Fig. 13). The positive anomalies are particularly well-defined over the southwestern part of the Indian Ocean during August and September, suggesting a weaker meridional pressure gradient over the domain and a northward shift of the monsoon trough, which is consistent with the rainfall composite map for these years (Fig. 8). The opposite SLP pattern develops in June and July of the years following the drought years but weakens in August and finally disappears in September, mainly because the negative SLP anomalies over Peninsular India and surrounding oceanic areas first decay in August and finally change sign and become positive in September (Fig. 12).

This discrepancy in the broad-scale SLP pattern suggests an explanation for the weaker consistency of the biennial rainfall pattern observed between the drought years and the years following them (Fig. 8). This is also consistent with the finding that SLP variations over Peninsular India and central Indian Ocean are strongly associated with LF fluctuations and suggests that the LF and B modes may be out of phase during the years succeeding to exceptional rainfall years.

The SST anomalies set up at the end of ISM of these succeeding years are generally weaker than those observed during fall of the drought and flood years and, in fact, disappear during the following winter season (figures not shown). Accordingly, the SLP B oscillation also disappears and no B characteristics or broad-scale anomaly patterns are apparent during the next ISMs.

7. Conclusions and discussion

Insights into the low-frequency variability of the monsoon systems have been derived by analyzing the space–time structure of SLP, SST, AT, and rainfall

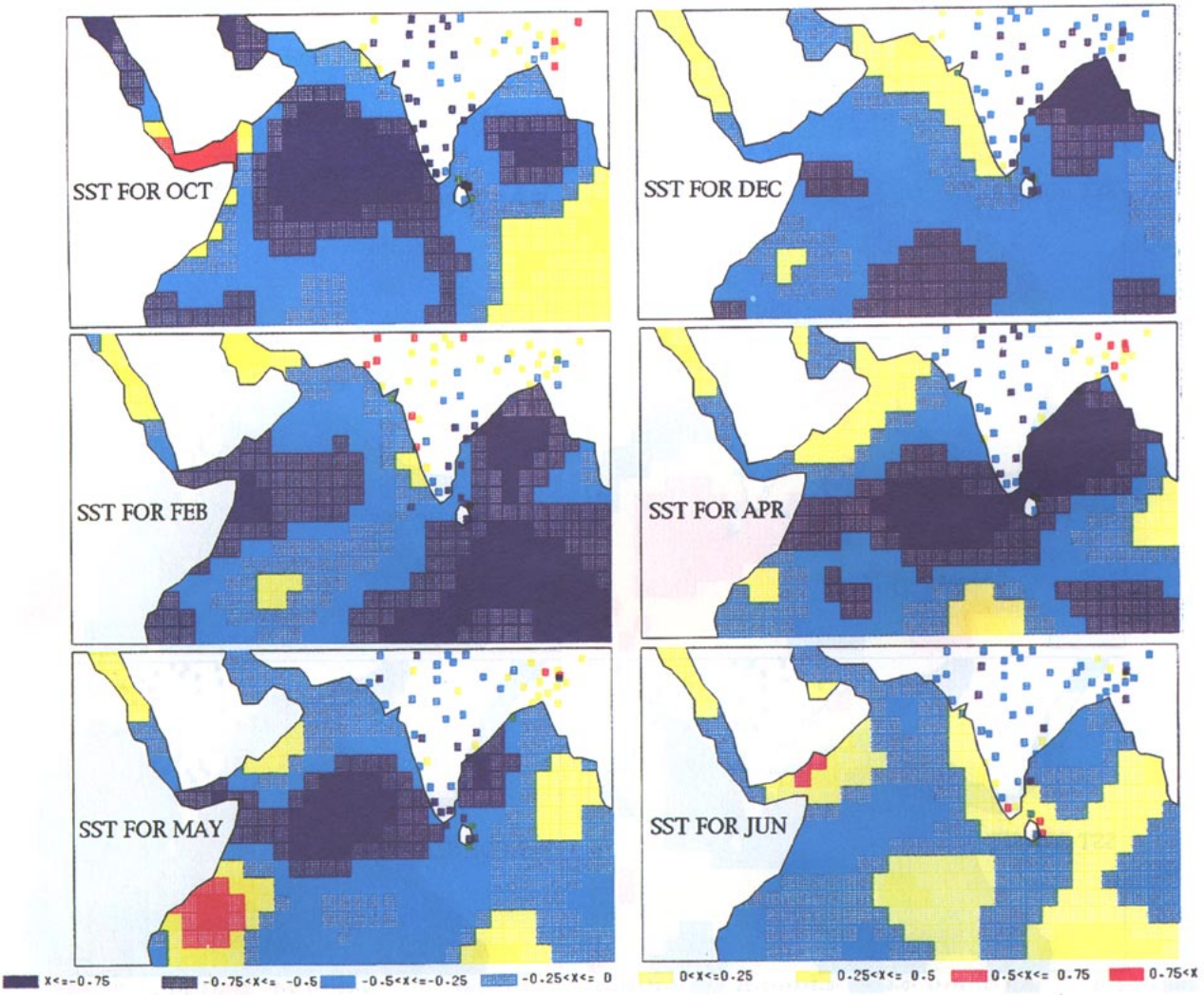

FIG. 11. SST and AT monthly normalized anomaly composites for October and December of eight heavy rainfall years and February, April, May, and June of the years following these heavy rainfall years.

monthly anomalies over the Indian Ocean and subcontinent since the turn of this century.

The analysis suggests the existence of two distinct modes of ISM circulation. The first induces rainfall anomalies on the west coast of India and in the Indo-Gangetic plains and the second is coupled with rainfall variations in the peninsula. The heavy or deficient rainfall ISMs are linked with the coupling of these two circulation modes.

Two interannual low-frequency oscillations (B—biennial and LF—low-frequency) constructively interfere to explain the intensity variations of these patterns of circulation anomaly. The major findings about these two frequency bands are given below.

A definite B oscillation exists on the SLP fields in the Indian areas. This B oscillation is unambiguously linked with a southwest–northeast SLP anomaly gradient. This B atmospheric cycle is a pure biennial mode in contrast to the quasibiennial appearance of this timescale over the Pacific (Rasmusson et al. 1990; Barnett 1991).

Although the phase of this B atmospheric cycle over the Indian Ocean is nearly constant throughout the period of study, its amplitude undergoes important swings. The more striking feature associated with this amplitude fluctuation of the B SLP pulses is the tendency for the energy associated with the B mode to decrease over the land while it increases steadily over the Indian Ocean from 1900 to 1970. This space–time behavior suggests that the forcing processes that sustain B variability over the Indian Ocean have varied somewhat during the 1900–1970 period.

During ISM, the SLP anomaly dipole associated with the B atmospheric oscillation can be interpreted as an expansion–contraction of the monsoon activity since this dipole is strongly coupled with rainfall vari-

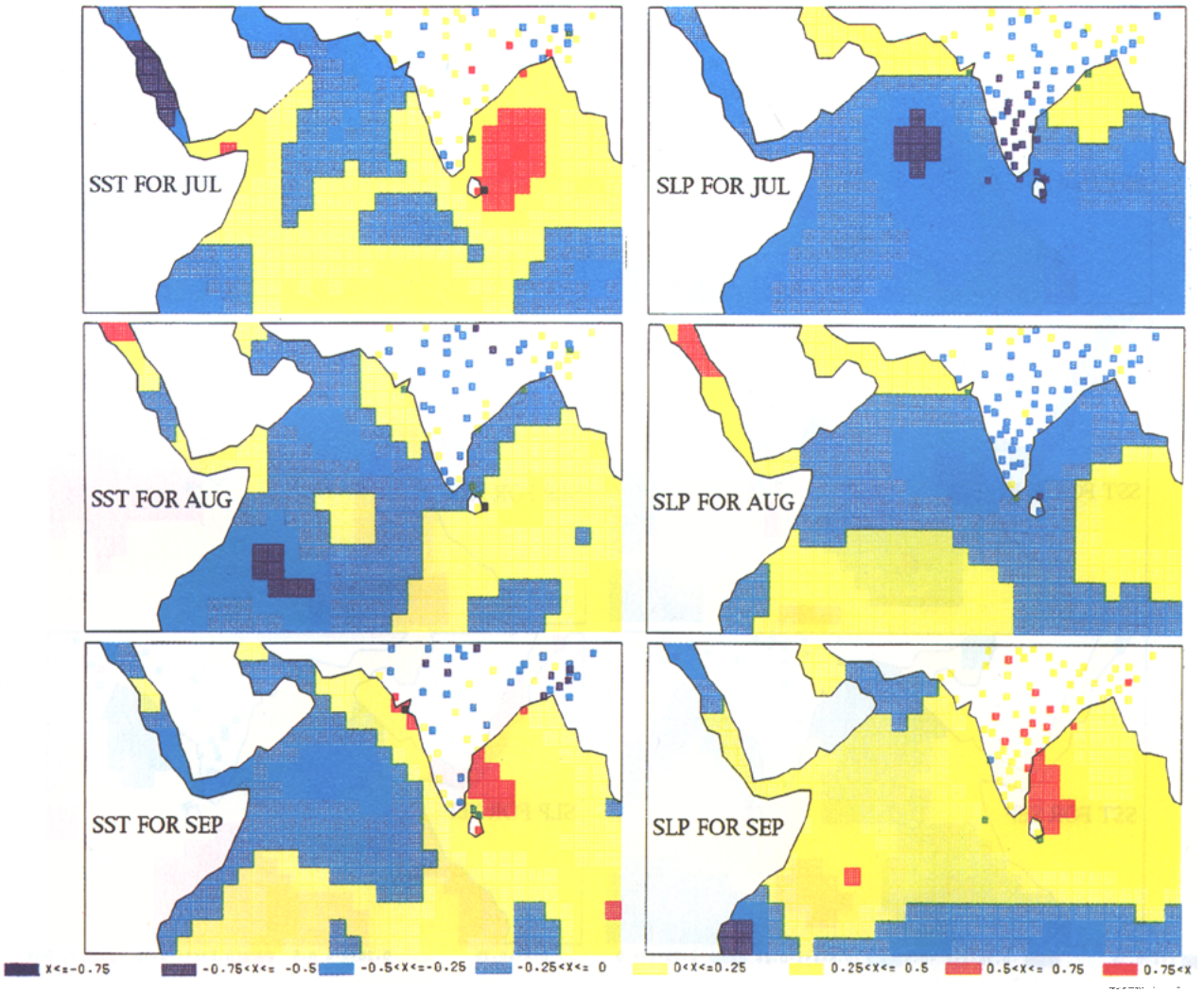

FIG. 12. SST, AT, and SLP monthly normalized anomaly composites for July, August, and September of the years following the deficient rainfall years.

ations over Peninsula. This B rhythm of monsoon circulation explained why Indian Ocean SST fields and the overlying atmosphere are mainly coupled at a B timescale, as suggested by cross-spectral computations, since the ocean surface layer is greatly influenced by wind-induced effects such as the decrease–increase of upwellings, wind mixing, cloudiness, and evaporation during ISM (Cadet and Diehl 1984; Joseph and Pillai 1984, 1986).

On the other hand, it is difficult to imagine some physical processes that can give rise to a B signal without some type of ocean forcing, particularly during recent decades when the B cycle is so sharply defined over the ocean and so weak over the continent. The results of a composite analysis support this hypothesis since the drought (flood) years are followed by relatively wet (dry) years and since it is observed that an SST anomaly produced by exceptional ISMs can indeed persist during the whole winter and may exert an influence on the next ISM.

First, it seems that the large and persistent cold (warm) SST and AT anomalies that followed the flood (drought) years can weaken (strengthen) the spring and earlier summer heating of both the landmasses and northern Indian Ocean, which is necessary for building up of the monsoon trough of the next ISM.

Second, there is some consistency in the space–time evolution of SST and SLP anomalies, suggesting that SST anomalies may force the broad-scale SLP anomaly pattern and hence determine the position of large-scale precipitation convergence zone during ISM of both exceptional rainfall years and years following them. These observations are broadly consistent with the Lindzen and Nigam hypothesis (1987), which postulates that surface temperature gradients are closely coupled with the SST gradient through turbulent vertical

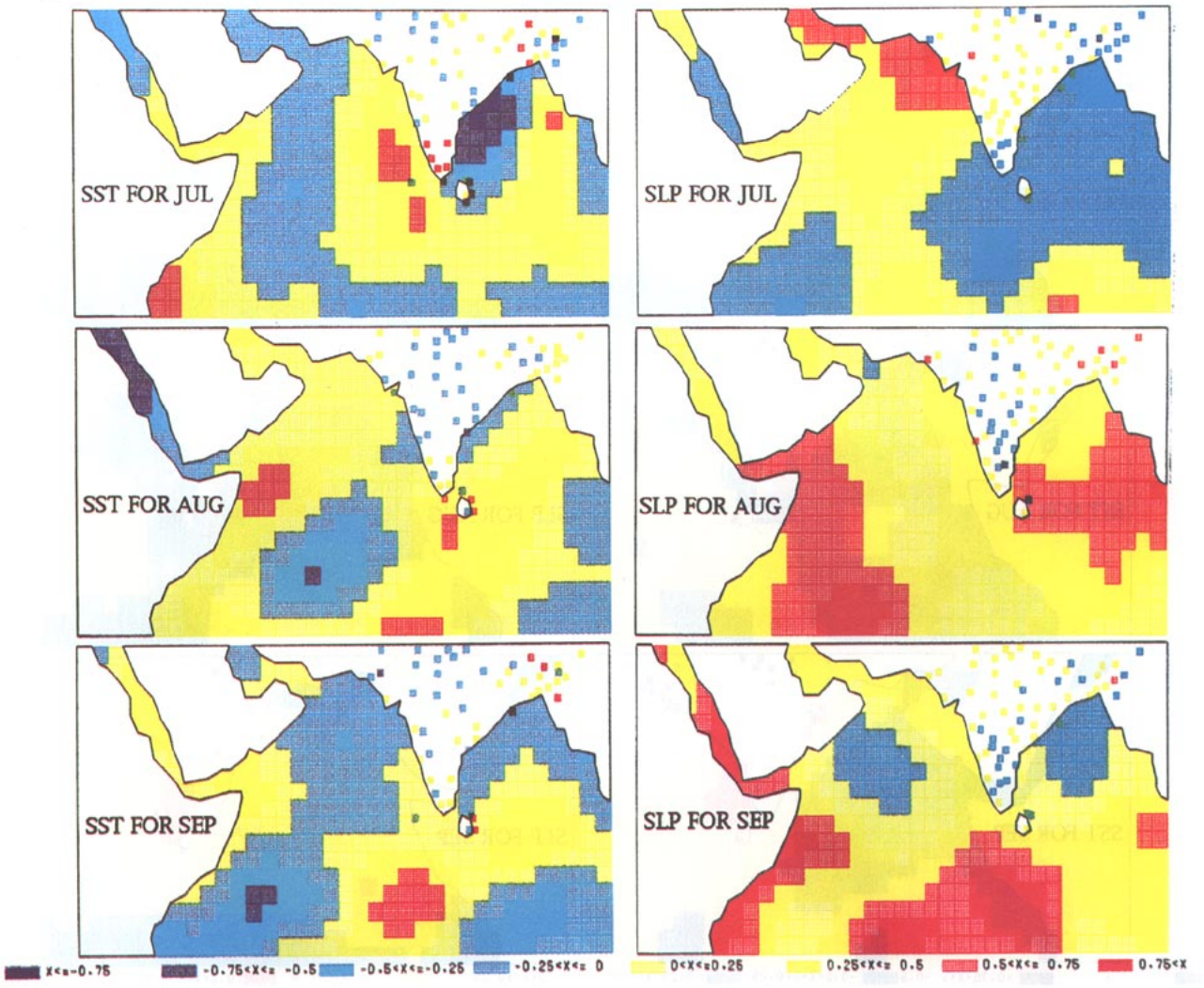

FIG. 13. Same as in Fig. 12, but for the years following the heavy rainfall years.

mixing in the Tropics and that these temperature gradients may force SLP gradients and hence set up the main convergence zones in the boundary layer. Since the broad-scale SST anomaly patterns during ISM of heavy or deficient rainfall years are globally opposite of those found during the succeeding years, the SST forcing will be also reversed and may then explain the observed B atmospheric and rainfall fluctuations.

Finally, if we refer to the SST climatology during ISM, the SST composites suggest a reversed variation of the ocean surface with a SST above 28°C in the central part of the Indian Ocean for the exceptional rainfall years and the years following them. This SST threshold is a necessary condition, though not sufficient, for large-scale deep convection to occur in monsoon areas (Gadgil et al. 1984; Graham and Barnett 1987). This other possible feedback of SST anomalies at the B timescale for sustaining or decreasing the convective activity over the Indian Ocean and subcontinent is well supported by the spatial characteristics associated with the B atmospheric oscillation since this spatial variability reflects a southwest–northeast translation of the monsoon trough in the context of ISM. The B nature of ISM rainfall over both Peninsular and northeast India for the heavy or deficient rainfall years and years following them also corroborates these speculations.

Many features in this composite analysis agree with the mechanisms postulated by Meehl (1993) for explaining B variability in the Tropics (e.g., strong air–sea coupling during the convective season with a SST forcing of one sign, a switch of sign of the SST anomalies at the end of this convective season, a persistence of these SST anomalies due to a very weak coupling between the ocean and the atmosphere during the winter season, and, finally, a new convective season starts but with a SST forcing of opposite sign that in turn will produce a new switch of sign of the SST anomalies at

the end of this convective season). However, while Meehl (1987, 1993) suggests that this B mechanism is more or less apparent a significant part of the time, our observations show that this mechanism is operating only between the exceptional monsoon years and the years following them, as far as the Indian monsoon areas are concerned, because the SST B oscillation rapidly fades away after the exceptional monsoon years. Indeed, no significant SST anomaly patterns are observed during the winter months preceding the heavy or deficient rainfall years even if strong SST anomaly dipoles are observed during ISM of these years, and spectral analysis does not show that the B timescale is the dominant mode of SST variations over the Indian Ocean.

Another discrepancy between the observations and Meehl's mechanism is that SLP anomalies and atmospheric responses to SST anomalies are not perfectly symmetric between the wet or dry years and the years following them. For example, the convergence anomalies, as determined by the SLP and rainfall anomalies, seem to feedback positively on the SST dipole pattern during exceptional rainfall years, while this positive feedback is not observed during ISM of the second year of the ocean–atmosphere B cycle. This may explain, at least partly, the weaker climatic anomalies observed during the second year of the cycle.

More importantly, the strong amplitude and regular increase of SLP anomalies over the peninsula and neighboring oceanic areas, which are observed during ISM of heavy and deficient rainfall years (especially the heavy rainfall years), suggest that the maxima of the LF atmospheric mode may occur during these years because the LF mode is particularly well-defined over these areas. But this will imply that the LF and B modes will be out of phase during the next year of the B cycle, and this seems also to contribute largely to the fact that the space–time evolution of the climatic anomalies between the two years of the B cycle is not perfectly reversed (especially for the years following the deficient rainfall years).

A strong LF mode with period spanning 4–6 years is also clearly seen on the SLP fields. The spatial mark of this mode is strikingly different from the dipole pattern associated with the B timescale since it is linked with a domainwide pattern of SLP variation. The spatial structure of this SLP LF mode in the Indian sector is similar, in all respect, with the Indian portion of the first CEOF of the LF-filtered SLP series for the whole Tropics given by Barnett (1991). This strong similarity suggests that this mode is more associated with the interannual variations of the east–west circulation than to the swings of the Hadley cell over the Indian Ocean.

The variance associated with this band is typically more important than the one observed for the B mode. As the B signal, this mode has undergone very important swings of amplitude during 1900–1970. This timescale was largely predominant during the first part of this century whereas it accounts for nearly the same amount of variance as the B band during recent decades.

This mode has also a strong influence on ISM rainfall fluctuations, particularly over the Ghats and in the Gangetic plains. These significant correlations suggest that the LF SLP signal also controls the intensity of the convective activity over India. Both bands are important for explaining the rainfall variations on the land.

Finally, it is very intriguing to note that although the SST fields over the Indian Ocean are also structured by this longer timescale, the ocean–atmosphere interactions associated with the LF mode seem weaker than those observed for the B mode.

All together, these results indicate that the forcing mechanisms related to the B and LF atmospheric modes may be quite different, but they also suggest that intensity and spatial distribution of ISM rainfall anomalies depend upon the coupling or decoupling of the B and LF atmospheric anomalies. This conceptual framework explains why some authors achieved amazingly exact statistical predictions of ISM rainfall during the 1950–1970 period (e.g., Kung and Sharif 1982; Wu 1985) since during this particular time interval, the LF and B modes were of great amplitude and have almost cyclical character in the Indian areas. Statistical rainfall predictions also indicated that the skill is much better for the forecasts during the second half of ISM than the whole ISM (Prasad and Singh 1992). Our analysis also gives some arguments for explaining this surprising situation since both the space and time amplitudes of the low-frequency oscillations seem higher at the end of ISM. Thus, forecast skill of monsoon rainfall over India is not linked to the persistence of isolated anomalous patterns of some meteorological parameters that occur randomly in time but to the existence of two slowly varying interannual low-frequency modes that exhibit some kind of cyclical space–time evolution.

As it stands now, the discovery of the physical processes that are responsible for the maintenance of the LF and B modes is of central interest for the long-range forecasting of ISM rainfall. It is our hope that this observational study will stimulate some simulation efforts in the climate community to explain physically the exact mechanisms sustaining the B cycle over the Indian Ocean.

Acknowledgments. The author is particularly grateful to Dr. D. L. Cadet for giving him most of the basic data products used in this study. Special thanks are also due to Prof. T. Yasunari for his comments and for the quiet time needed to prepare this paper. The two anonymous reviewers' comments were extremely helpful in the revision of the paper. Some of the results presented in this paper represent part of the author's Ph.D. supported by a grant-in-aid obtained through Université Paris VII (département de Géographie), France. Most of the processing has been done at Laboratoire de Mé-

téorologie Dynamique (CNRS, Palaiseau, France) and the author acknowledges Dr. Sadourny for these computing facilities. This research was also supported in part by a Grant-in-Aid for Scientific Research from the Ministry of Education and Culture of Japan for 1993.

APPENDIX

Work Notes on EOF Analysis with Missing Values in the Data

a. *Minimization of the $f(\mathbf{Y})$ functional in the incomplete case*

In order to show how the $f(\mathbf{Y})$ functional (7) can be minimized in the incomplete case, we restate first the Eckart-Young theorem in an equivalent form. For any $p \times n$ real matrix $\mathbf{X}$ with representation (1) and any integer $q \leq p$, the minimum of

$$\|\mathbf{X} - \mathbf{Y}\|^2 = f(\mathbf{Y}) \tag{A1}$$

on all $p \times n$ matrix $\mathbf{Y}$ of rank less than q is equal to the minimum of

$$\|\mathbf{X} - \mathbf{AB}\|^2 = f_1(\mathbf{A}, \mathbf{B}) \tag{A2}$$

on all $p \times q$ matrix $\mathbf{A}$ and $q \times n$ matrix $\mathbf{B}$. Moreover, when this minimum is attained, we must also have

$$\mathbf{AB} = \hat{\mathbf{X}}^q = \mathbf{U}_q \mathbf{\Sigma}_q \mathbf{V}_q^t.$$

A proof of the equivalence of these two matrix forms of the Eckart–Young theorem can be found in Gabriel (1978). Correspondingly, it is not difficult to show that the minimum of $f(\mathbf{Y})$ is equivalent to the minimum of

$$f_1(\mathbf{A}, \mathbf{B}) = \sum_{ij} (\mathbf{X}_{ij} - \sum_{k=1}^{q} \mathbf{A}_{ik}\mathbf{B}_{kj})^2 \tag{A3}$$

in the incomplete case. Moreover, when this minimum is achieved we must also have $\mathbf{Y} = \mathbf{AB}$. Thus, it is equivalent to minimize $f(\mathbf{Y})$ or $f_1(\mathbf{A}, \mathbf{B})$ in both the complete and incomplete cases.

Now let us consider in some details how the nonlinear least-squares minimization problem (A3) can be solved in the incomplete case. The only one restriction we imposed on $\mathbf{X}$ for this problem to be solved is that this matrix must have at least one nonmissing element in each line and column. We first introduce some notations.

- For all $\alpha \in \Re^p$, the symbol $\text{diag}(\alpha)$ is used to represent a diagonal $p \times p$ matrix with diagonal elements, $\text{diag}(\alpha)_{jj}$, equal to α_j.
- For any $\mathbf{U}$ matrix, the symbol $\mathbf{U}_{\cdot j}$ is used to represent the jth column vector of the $\mathbf{U}$ matrix.
- For any $\mathbf{U}$ matrix, the symbol $\mathbf{U}^+$ represents the pseudo inverse of $\mathbf{U}$ (see Lawson and Hanson 1974, 36).
- For any $\mathbf{U}$ and $\mathbf{V}$ matrices, the symbol $\mathbf{U}\#\mathbf{V}$ is used to mean the element by element product of the $\mathbf{U}$ and $\mathbf{V}$ matrices: $[\mathbf{U}\#\mathbf{V}]_{ij} = \mathbf{U}_{ij} \cdot \mathbf{V}_{ij}$.

Then (A3) may be rewritten as

$$f_1(\mathbf{A}, \mathbf{B}) = \sum_{i=1}^{p} \sum_{j=1}^{n} \mathbf{W}_{ij}(\mathbf{X}_{ij} - \sum_{k=1}^{q} \mathbf{A}_{ik}\mathbf{B}_{kj})^2, \tag{A4}$$

where $\mathbf{W}$ is a presence–absence matrix (e.g., $\mathbf{W}_{ij} = 1$ if $\mathbf{X}_{ij}$ is observed and $\mathbf{W}_{ij} = 0$ if $\mathbf{X}_{ij}$ is missing). With the notations introduced above, (A4) becomes

$$\begin{aligned} f_1(\mathbf{A}, \mathbf{B}) &= \|\mathbf{W}\#(\mathbf{X} - \mathbf{AB})\|^2 \\ &= \sum_{j=1}^{n} \|\mathbf{W}_{\cdot j}\#(\mathbf{X}_{\cdot j} - \mathbf{AB}_{\cdot j})\|^2 \\ &= \sum_{j=1}^{n} \|(\mathbf{W}_{\cdot j}\#\mathbf{X}_{\cdot j}) - (\text{diag}(\mathbf{W}_{\cdot j})\mathbf{A})\mathbf{B}_{\cdot j}\|^2. \end{aligned} \tag{A5}$$

With this formulation of our nonlinear least-squares problem, we observe that the best choice of $\mathbf{B}$ for a given $\mathbf{A}$ matrix is obtained by solving n independent linear least squares problems. Using the pseudo inverse of the $[\text{diag}(\mathbf{W}_{\cdot j})\mathbf{A}]$ matrix, $\mathbf{B}_{\cdot j}$ (for $j = 1, \cdots, n$) can therefore be calculated by

$$\mathbf{B}_{\cdot j} = [\text{diag}(\mathbf{W}_{\cdot j})\mathbf{A}]^+(\mathbf{W}_{\cdot j}\#\mathbf{X}_{\cdot j}) \tag{A6}$$

(see Lawson and Hanson 1974, 37). Inserting now (A6) into (A5), we obtain a new nonlinear functional involving only the $\mathbf{A}$ matrix

$$\begin{aligned} f_2(\mathbf{A}) = \sum_{j=1}^{n} \|\{\mathbf{I}_p - [\text{diag}(\mathbf{W}_{\cdot j})\mathbf{A}] \\ \times [\text{diag}(\mathbf{W}_{\cdot j})\mathbf{A}]^+\}(\mathbf{W}_{\cdot j}\#\mathbf{X}_{\cdot j})\|^2. \end{aligned} \tag{A7}$$

This modified functional can be termed a variable projection functional since the matrix in braces is an orthogonal projector involving only the $\mathbf{A}$ variable (Golub and Pereyra 1973). Equation (A7) shows that the minimization of $f_1(\mathbf{A}, \mathbf{B})$ can be separated in two steps. Once a $\mathbf{A}$ matrix has been obtained by minimizing $f_2(\mathbf{A})$, the $\mathbf{B}$ matrix can be obtained by an application of (A6). The rational for employing this separation of variables to minimize $f_1(\mathbf{A}, \mathbf{B})$ is given by a theorem proved by Golub and Pereyra (1973). This theorem shows under some differentiability conditions that if $\hat{\mathbf{A}}$ is a critical point (or a global minimizer) of $f_2(\mathbf{A})$ and $\hat{\mathbf{B}}$ is calculated by (A6), then $(\hat{\mathbf{A}}, \hat{\mathbf{B}})$ is a critical point (or a global minimizer) of $f_1(\mathbf{A}, \mathbf{B})$.

Methods for minimizing (A7) are termed variable projection algorithms and are given by Golub and Pereyra (1973), Kaufman (1975), and Ruhe and Wedin (1980). Their advantages are that they usually solve mixed linear–nonlinear least-squares problems like (A3) in less time and fewer function evaluations

than standard nonlinear least squares codes and that no starting estimate of the linear variable **B** is required (this last point is particularly important here, see below).

In any of the missing EOF analyses presented in this paper, the Euclidean norm of the gradient of the functional $f_1(\mathbf{A}, \mathbf{B})$ has been reduced by many orders of magnitude (see Table A1), thereby suggesting that at least a local minimum of the functional $f_1(\mathbf{A}, \mathbf{B})$ has been obtained in each case.

b. Estimation of principal components, spatial loading vectors, and amounts of variance explained by each principal component

After $f_1(\mathbf{A}, \mathbf{B})$ is minimized, we have just to compute the SVD of the **AB** product for estimating the principal components, the loading vectors and the eigenvalues of the missing EOF analysis. Let

$$\mathbf{AB} = \hat{\mathbf{U}}_q \hat{\Sigma}_q \hat{\mathbf{V}}_q^t$$

be the SVD of **AB**. Then the estimated principal components are just $\hat{\mathbf{V}}_q$ and the estimated spatial loadings may be defined as $\hat{\mathbf{U}}_q \hat{\Sigma}_q$ if the lines and columns of **X** referred to stations and time observations, respectively. These estimated spatial loadings can be thought as estimates of the correlations between the stations time series and the principal components as in the traditional EOF analysis.

Finally, to get some estimate of the percentage of variance explained by each principal component of the missing EOF model from the singular values, λ_k, of the **AB** product, we can form the statistics

$$I_k = (\lambda_k^2/n)/(\sum_{i=1}^{p} (\sum_{j=1}^{n} \mathbf{W}_{ij}\mathbf{X}_{ij}^2)/(\sum_{j=1}^{n} \mathbf{W}_{ij})) \quad \text{for} \quad 1 \leq k \leq q. \quad \text{(A8)}$$

The numerator in the right-hand side of (A8) represents the variance of the kth estimated principal component, while the denominator is the sum of the variance of the p variables estimated by using all the available data values. The mutual consistency of these q individual statistical estimates can be checked with the following statistic:

$$I_{\text{tot}} = \|\mathbf{W}\#\mathbf{AB}\|^2/\|\mathbf{W}\#\mathbf{X}\|^2. \quad \text{(A9)}$$

This last ratio gives the true percentage of the total variance explained by the q principal components model in the incomplete case. This important geometrical property holds since it is readily observed that we have the equality

$$\|\mathbf{W}_{\cdot j}\#\mathbf{X}_{\cdot j}\|^2 = \|\mathbf{W}_{\cdot j}\#\mathbf{AB}_{\cdot j}\|^2 + \|\mathbf{W}_{\cdot j}\#(\mathbf{X}_{\cdot j} - \mathbf{AB}_{\cdot j})\|^2 \quad \text{(A10)}$$

for $j = 1$ to n, when $\mathbf{B}_{\cdot j}$ is computed by (A6). By summing all these equalities for $j = 1$ to n, we obtain

$$\|\mathbf{W}\#\mathbf{X}\|^2 = \|\mathbf{W}\#\mathbf{AB}\|^2 + \|\mathbf{W}\#(\mathbf{X} - \mathbf{AB})\|^2. \quad \text{(A11)}$$

The left-hand side of (A11) is the total variance of the incomplete matrix **X**, while the first term in the right-hand side is the variance of **X** explained by the q principal components model. Consequently, (A9) gives the true fraction of the variance of **X** described by the missing EOF analysis with q components, as anticipated above. As an illustration, the quantities I_k, I_{tot} obtained at the output of the variable projection algorithms for the analyses described in this paper are given in Table A1.

c. Estimating the number q of principal components before the missing EOF analysis

Another difficulty in the missing EOF analysis is that the number of principal components of the model has to be fixed a priori. Indeed, it seems quite difficult to choose this important parameter without any knowledge about the cross-products (or covariance or correlation) matrix $\mathbf{XX}^t$ (or $\mathbf{X}^t\mathbf{X}$) and its spectrum.

However, efficient methods for estimating this cross-products matrix in presence of missing values exist in the literature (Der Megreditchian 1988). From these estimations, the problem of choosing the q parameter is quite similar to the problem of determining the number of significant eigenvalues of a correlation or covariance matrix. Standard tests (e.g., Overland and Pre-

TABLE A1. Results of the missing EOF analyses of the rainfall and SLP fields over the Indian subcontinent during 1900–1970. The line labeled SLP (1–12) gives the results of the SLP EOF analysis computed on all the calendar monthly fields from January to December while the lines SLP (6–9) and rainfall (6–9) show the results of the SLP and rainfall analyses computed on the summer monthly fields (June to September) only. Here I_1, I_2, and I_3 are statistical estimates of the percentages of variance accounted for by the two or three estimated eigenmodes for each analysis. Term I_{tot} gives the true percentage of variance accounted for by the missing EOF models with two or three components. Der and Iter give the norm of the gradient of the functional $f_1(\mathbf{A}, \mathbf{B})$ and the number of iterations after the convergence of the variable projection algorithms used to minimize f_1 (**A**, **B**). See the appendix for details.

Variable	I_1	I_2	I_3	I_{tot}	Der	Iter
SLP (1–12)	64.9%	10.9%	—	74.8%	0.008	14
SLP (6–9)	53.2%	18.6%	5.2%	79.0%	0.01	20
Rainfall (6–9)	13.2%	8.6%	—	21.2%	0.001	15

isendorfer 1982), as well as empirical rules, have been used here for making the "right" choice in the various missing EOF analyses.

It should be noted that the estimated $\mathbf{X} \cdot \mathbf{X}'$ matrix can furnish another useful information after this preliminary step of the analysis, because the q first eigenvectors of this matrix turn out to be a very good starting point for the variable projection algorithms used in minimizing $f_2(\mathbf{A})$. Technical tests have shown that the use of this first-guess speeds up considerably the convergence of the algorithms used here if the q parameter has been determined in a responsible manner.

REFERENCES

Barnett, V., and T. Lewis, 1978: *Outliers in Statistical Data.* John Wiley & Sons, 451 pp.

Barnett, T. P., 1991: The interaction of multiple timescales in the tropical climate system. *J. Climate,* **4,** 269–285.

Bhalme, H. N., and D. A. Mooley, 1980: Large-scale droughts–floods and monsoon circulation. *Mon. Wea. Rev.,* **108,** 1197–1211.

——, and S. K. Jadhav, 1984: The Southern Oscillation and relation to the monsoon rainfall. *J. Climatol.,* **4,** 509–520.

Blanford, H. F., 1884: On the connexion of the Himalaya snowfall and seasons of drought in India. *Proc. Roy. Soc. London,* **37,** 3–22.

Bottomley, M., C. K. Folland, J. Hsiung, R. E. Newell, and D. E. Parker, 1990: Global ocean surface temperature atlas "GOSTA." Joint project of the U.K. Meteorological Office and Massachusetts Institute of Technology, 20 pp., 313 plates, HMSO.

Cadet, D. L., 1985: The Southern Oscillation over the Indian Ocean. *J. Climatol.,* **5,** 189–212.

——, and B. C. Diehl, 1984: Interannual variability of surface fields over the Indian Ocean during recent decades. *Mon. Wea. Rev.,* **112,** 1925–1935.

Der Megreditchian, G., 1988: Problèmes engendrés par les données manquantes dans la pratique statistique. Note de travail de l'EERM n°28 (in French). Ecole Nationale de la Météorologie, 75007 Paris, 39 pp.

Elliott, W. P., and J. K. Angell, 1987: The relation between Indian monsoon rainfall, the Southern Oscillation, and hemispheric air and sea temperature 1884–1984. *J. Climate Appl. Meteor.,* **26,** 943–948.

——, and ——, 1988: Evidence for changes in Southern Oscillation relationships during the last 100 years. *J. Climate,* **1,** 729–737.

Gabriel, K. R., 1978: Least squares approximation of matrices by additive and multiplicative models. *J. Roy. Statist. Soc.,* B, **40,** 186–196.

Gadgil, S., P. V. Joseph, and N. V. Joshi, 1984: Ocean–atmosphere coupling over monsoon regions. *Nature,* **312,** 141–143.

Golub, G. H., and V. Pereyra, 1973: The differentiation of pseudo-inverses and non-linear least squares problems whose variables separate. *SIAM J. Num. Anal.,* **10,** 413–432.

Graham, N. E., and T. P. Barnett, 1987: Sea surface temperature, surface wind divergence, and convection over tropical oceans. *Science,* **238,** 657–659.

Horel, J. D., 1981: A rotated principal component analysis of the interannual variability of the Northern Hemisphere 500-mb height field. *Mon. Wea. Rev.,* **109,** 2080–2092.

Jalickee, J. B., and D. R. Hamilton, 1977: Objective analysis and classification of oceanographic data. *Tellus,* **29,** 545–560.

Joseph, P. V., and P. V. Pillai, 1984: Air–sea interaction on a seasonal scale over north Indian Ocean. Part I: Interannual variations of sea surface temperature and Indian summer monsoon rainfall. *Mausam,* **35,** 323–330.

——, and ——, 1986: Air–sea interaction on a seasonal scale over north Indian Ocean. Part II: Monthly mean atmosphere and oceanic parameters during 1972 and 1973. *Mausam,* **37,** 159–168.

Kaufman, L., 1975: Variable projection method for solving separable nonlinear least squares problems. *BIT,* **15,** 49–57.

Krishnamurti, T. N., H. S. Bedi, and M. Subramaniam, 1971: The summer monsoon of 1987. *J. Climate,* **2,** 321–341.

Kung, E. C., and T. A. Sharif, 1982: Long-range forecasting of the Indian summer monsoon onset and rainfall with upper air parameters and sea surface temperature. *J. Meteor. Soc. Japan,* **60,** 672–681.

Kutzbach, J. E., 1967: Empirical eigenvectors of sea level pressure, surface temperature, and precipitation complexes over North America. *J. Appl. Meteor.,* **6,** 791–802.

Lawson, C. L., and R. J. Hanson, 1974: *Solving Least Squares Problems.* Prentice-Hall, 315 pp.

Lindzen, R. S., and S. Nigam, 1987: On the role of sea surface temperature gradients in forcing low-level winds and convergence in the Tropics. *J. Atmos. Sci.,* **44,** 2418–2436.

Meehl, G. A., 1987: The annual cycle and its relationships to interannual variability in the tropical Pacific and Indian regions. *Mon. Wea. Rev.,* **115,** 27–50.

——, 1993: A coupled air–sea biennial mechanism in the tropical Indian and Pacific regions: Role of the ocean. *Mon. Wea. Rev.,* **6,** 31–41.

Overland, J. E., and R. W. Preisendorfer, 1982: A significance test for principal components applied to cyclone climatology. *Mon. Wea. Rev.,* **110,** 1–4.

Parthasarathy, B., and D. A. Mooley, 1978: Some features of a long homogeneous series of Indian summer monsoon rainfall. *Mon. Wea. Rev.,* **106,** 771–781.

——, and G. B. Pant, 1985: Seasonal relationships between Indian summer monsoon rainfall and the Southern Oscillation. *J. Climatol.,* **5,** 369–378.

——, N. A. Sontakke, A. A. Monot, and D. R. Kothawale, 1987: Droughts/floods in the summer monsoon season over different meteorological subdivisions of India for the period 1871–1984. *J. Climatol.,* **7,** 57–70.

Prasad, K. D., and S. V. Singh, 1988: Monsoon rainfall and Southern Oscillation responses in the pressures over the Northern Indian Ocean. *Adv. Atmos. Sci.,* **5,** 243–251.

——, and ——, 1992: Possibility of predicting Indian monsoon rainfall on reduced spatial and temporal scales. *J. Climate,* **5,** 1357–1361.

Ramesh Babu, V., M. Subba Rao, and M. V. Rao, 1989: Influence of eastern Arabian Sea on summer monsoon rainfall over west coast of India. *Vayu Mandal,* July–December 1989, 75–78.

Rao, K. G., and B. N. Goswami, 1988: Interannual variations of sea surface temperature over the Arabian Sea and the Indian monsoon: A new perspective. *Mon. Wea. Rev.,* **116,** 558–568.

Rasmusson, E. M., and T. H. Carpenter, 1983: The relationship between eastern equatorial Pacific sea surface temperatures and rainfall over India and Sri Lanka. *Mon. Wea. Rev.,* **111,** 517–528.

——, X. Wang, and C. F. Ropelewski, 1990: The biennial component of ENSO variability. *J. Mar. Sci.,* **1,** 71–96.

Richman, M. B., 1986: Review article, rotation of principal components. *J. Climatol.,* **6,** 293–335.

Ropelewski, C. F., M. S. Halpert, and X. Wang, 1992: Observed tropospheric biennial variability and its relationship to the Southern Oscillation. *J. Climate,* **5,** 594–614.

Ruhe, A., and P. A. Wedin, 1980: Algorithms for separable nonlinear least squares problems. *SIAM Rev.,* **22,** 318–337.

Shukla, J., 1987: Interannual variability of monsoons. *Monsoons,* J. S. Fein and P. L. Stephens, Eds., John Wiley & Sons, 339–463.

——, and B. M. Misra, 1977: Relationships between sea surface temperature and wind speed over the central Arabian Sea and monsoon rainfall over India. *Mon. Wea. Rev.,* **105,** 798–1002.

——, and D. A. Paolino, 1983: The Southern Oscillation and long-range forecasting of the summer monsoon rainfall over India. *Mon. Wea. Rev.*, **111,** 1830–1837.

Spangler, W. M. L., and R. L. Jenne, 1984: World Monthly Surface Station Climatology. [Available from NCAR, Scientific Computing Division, Boulder, CO, 80307, USA].

Terray, P., 1992: Interannual variability of Indian summer monsoon and long-range forecasting of rainfall over India. Ph.D. dissertation, University Paris VII, Paris (in French) [Available from Laboratoire de Météorologie du CNRS, Ecole Polytechnique, 91128 Palaiseau Cedex, France.]

——, 1994: An evaluation of climatological data in the Indian Ocean area. *J. Meteor. Soc. Japan.*, **72,** 359–386.

Trenberth, K. E., and D. J. Shea, 1987: On the evolution of the Southern Oscillation. *Mon. Wea. Rev.*, **115,** 3078–3096.

U.S. Weather Bureau, 1961–1984: Monthly Climatic Data for the World. ESSA/NOAA.

Walker, G. T., 1923: Correlation in seasonal variations of weather VIII. Memoirs Indian Meteorological Dept. 24, 75–131.

Weare, B., 1979: A statistical study of the relationships between ocean surface temperatures and the Indian monsoon. *J. Atmos. Sci.*, **36,** 2279–2291.

Wu, M. C., 1985: On the prediction of the Indian summer monsoon. *Pap. Meteor. Res.*, **8,** 34–44.

——, and S. Hastenrath, 1986: On the interannual variability of the Indian monsoon and the Southern Oscillation. *Arch. Meteor. Geophys. Bioklimatol.*, Serie B, **36,** 239–261.

Yasunari, T., 1990: Impact of Indian monsoon on the coupled atmosphere/ocean system in the tropical Pacific. *Meteor. Atmos. Phys.*, **44,** 29–41.

——, 1991: The monsoon year—a new concept of the climatic year in the Tropics. *Bull. Amer. Meteor. Soc.*, **72,** 1331–1338.